


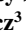


## Ocean Circulation Near Cape Hatteras: Observations of Mean and Variability

Lu Han<sup>1</sup> , Harvey Seim<sup>1</sup>, John Bane<sup>1</sup> , Dana Savidge<sup>2</sup>, Magdalena Andres<sup>3</sup> ,  
Glen Gawarkiewicz<sup>3</sup> , and Mike Muglia<sup>4</sup> 

<sup>1</sup>University of North Carolina, Chapel Hill, NC, USA, <sup>2</sup>Skidaway Institute of Oceanography, Savannah, GA, USA, <sup>3</sup>Woods Hole Oceanographic Institution, Woods Hole, MA, USA, <sup>4</sup>Coastal Studies Institute, East Carolina University, Wanchese, NC, USA

### Key Points:

- The time-mean depth-averaged shelf and shelfbreak currents are mostly aligned with isobaths and oriented toward Cape Hatteras
- On average, the open-ocean water intrudes on the shelf south of The Point while the shelf water exports to the open ocean north of The Point
- Wind-driven along-shelf flow pattern and Gulf Stream-driven convergent flow pattern are predominant in the shelf velocity field

### Correspondence to:

L. Han,  
luhan@unc.edu

### Citation:

Han, L., Seim, H., Bane, J., Savidge, D., Andres, M., Gawarkiewicz, G., & Muglia, M. (2022). Ocean circulation near Cape Hatteras: Observations of mean and variability. *Journal of Geophysical Research: Oceans*, 127, e2022JC019274. <https://doi.org/10.1029/2022JC019274>

Received 9 SEP 2022  
Accepted 16 NOV 2022

**Abstract** The convergence of different water masses on the shelf and along the shelfbreak, and cross-isobath shelf-open ocean exchanges contribute to the complex circulation near Cape Hatteras. We examine the mean and variability of these circulations using data from nine bottom-mounted acoustic Doppler current profilers, deployed over the mid- to outer-continental shelf north and south of Cape Hatteras as part of the Processes driving Exchange At Cape Hatteras program. The 18-month-mean depth-averaged shelf flows are mostly aligned with isobaths and oriented toward Cape Hatteras. At two sites just north of Cape Hatteras, mean flows have a strong cross-shelf component. Two dominant spatial patterns in the velocity field are obtained from an empirical orthogonal function analysis. The two leading modes contain 61% of the total variance. The spatial variation of Mode 1 exhibits an along-shelf flow pattern, while that of Mode 2 shows a convergent flow pattern. The principal component (PC) series of Mode 1 is significantly correlated with the local wind stress, confirming that the along-shelf flow is wind-driven as expected. The PC of Mode 2 is highly correlated with the Gulf Stream lateral position as inferred from the current- and pressure-sensor-equipped inverted echo sounders over the slope south of Cape Hatteras, which indicates that Gulf Stream movement drives time-varying shelf flow convergence. Conditionally averaged sea-surface temperature and high-frequency radar-measured surface currents based on PC1 and PC2 confirm these relationships and further illustrate how the wind and Gulf Stream forcing work together to influence the flow regime in this region.

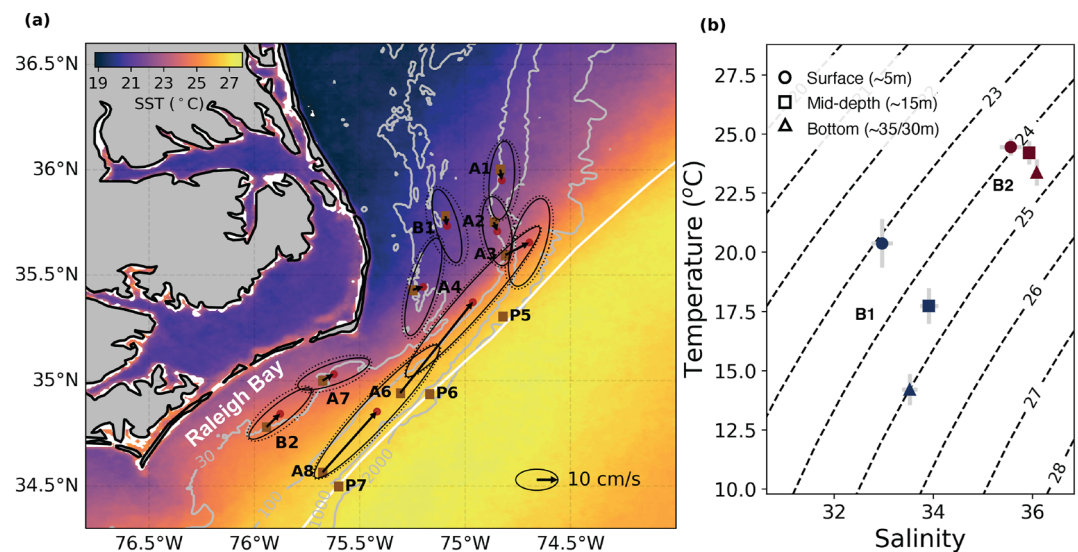
**Plain Language Summary** Several oceanographic processes occur within a small geographic area east of Cape Hatteras. Cool and warm ocean currents meet and collide on the continental shelf, resulting in complex exchange between the shelf and the adjacent open ocean. To better characterize the complicated circulation and understand the processes driving exchanges in this region, we analyze 18-month current velocity data from an observational array deployed near Cape Hatteras on the shelf and the neighboring continental slope. The time-mean circulation is characterized as converging flows both on the shelf and along the shelfbreak. We find two dominant spatial patterns in the current velocity: a wind-driven along-shelf flow pattern and a Gulf Stream-driven convergent flow pattern. Additionally, the combined effect of the wind and Gulf Stream forcings mainly drives the shelf and open ocean exchanges.

## 1. Introduction and Background

Many oceanographic processes occur in the vicinity of Cape Hatteras USA, and together contribute to the complex flow regime there. Cape Hatteras and its sub-surface offshore extension, Diamond Shoals, mark the separation of the continental shelf along the U.S east coast into two distinct regions: South Atlantic Bight (SAB) and Mid Atlantic Bight (MAB). Like the coastline, the shelfbreak (~100-m isobath) changes its orientation from south to north, turning from about SW–NE to almost S–N at the “The Point,” offshore of Cape Hatteras near 35.5°N (Figure 1a). The Point is where the Gulf Stream typically separates from the continental margin, and it is also usually the southernmost detachment location of the Shelfbreak Jet (Csanady & Hamilton, 1988; Gawarkiewicz et al., 2008). On the adjacent continental shelf, both the MAB and SAB shelf waters generally flow toward Cape Hatteras. To better understand the seawater exchange between the continental shelf and the adjacent open ocean in this region, an integrated observational and modeling program, Processes driving Exchange At Cape Hatteras (PEACH; Andres, 2021; Han et al., 2021; Seim et al., 2022) was conducted in 2017–2018.

© 2022. The Authors.

This is an open access article under the terms of the [Creative Commons Attribution-NonCommercial-NoDerivs License](https://creativecommons.org/licenses/by-nc-nd/4.0/), which permits use and distribution in any medium, provided the original work is properly cited, the use is non-commercial and no modifications or adaptations are made.



**Figure 1.** (a) Mean depth-averaged flow and standard deviation ellipses at the processes driving exchange at Cape Hatteras (PEACH) moorings overlaid on the mean Sea Surface Temperature during PEACH period (April 2017–November 2018). The brown squares mark the locations of the moorings and three current- and pressure-sensor-equipped inverted echo sounders. The centers of the ellipses are marked as red dots and are located at the tip of each corresponding mean flow vector. The dashed ellipses are computed from the unfiltered hourly data, and the solid ellipses are from 40-hr low-pass filtered data. The mean flows computed from unfiltered and filtered data are nearly identical. The white contour shows the mean Gulf Stream position during PEACH derived from the 25-cm Sea Surface Height contour. (b) Mean temperature and salinity measured by three CTDs at each of B1 (blue) and B2 (red). Error bars are standard errors, dashed contours are potential density-1,000 in  $\text{kg}/\text{m}^3$ .

Prior to PEACH, results of three earlier studies formed the basic understanding of circulation near Cape Hatteras, including the major features and their relation to relevant forcings. These field programs comprised a Minerals Management Service-sponsored program in 1992–1994 (MMS study, Berger et al., 1995), the Department of Energy-funded “Ocean Margins Program” in 1996 (OMP, Verity et al., 2002), and the NSF-funded “Frontal Interactions Near Cape Hatteras” program in 2004–2005 (FINCH, Gawarkiewicz et al., 2008; Savidge & Austin, 2007). Along the MAB shelfbreak, the Shelfbreak Front separates MAB shelf waters from slope waters and along with the associated Shelfbreak Jet, is normally found near the  $\sim 100$  m isobath at  $39.5^\circ\text{N}$  (Forsyth et al., 2020). The Shelfbreak Jet carries  $\sim 0.3$  Sv of cold and fresh water from as far north as the Labrador Sea (Chapman & Beardsley, 1988; Fratantoni & Pickart, 2007; Gawarkiewicz et al., 2008; Linder & Gawarkiewicz, 1998) and exports this water to the open ocean north of Cape Hatteras typically between  $\sim 35.5^\circ$  and  $\sim 37^\circ\text{N}$  (Gawarkiewicz & Linder, 2006), as the front and jet are deflected offshore. Much of the MAB shelf water also has high latitude origins, with a low temperature and salinity (Chapman & Beardsley, 1988). On the MAB shelf inshore of the Shelfbreak Jet, the along-shelf transport is on the order of 0.1 Sv throughout the year (Churchill & Berger, 1998; Churchill & Gawarkiewicz, 2012, 2014; Savidge & Bane, 2001; Savidge & Savidge, 2014), and it decreases from north to south (Townsend et al., 2006) as the MAB water is diverted offshore en route to Cape Hatteras (Churchill & Gawarkiewicz, 2012). Mean poleward transport of about 0.08 Sv along the northern SAB delivers warm and salty SAB shelf water to Cape Hatteras, where it converges with MAB shelf water and forms the Hatteras Front (Savidge & Savidge, 2014).

The Gulf Stream undergoes a striking change near Cape Hatteras where the current leaves the shelf edge and upper continental slope and begins the transition from a topographically constrained western boundary current to a vigorously meandering free jet (Andres, 2016). Downstream of its separation from the continental margin, the Gulf Stream meanders with longer periods and larger amplitudes than typically observed upstream of the separation (Savidge, 2004). The Gulf Stream's variability has been recognized as an important forcing agent affecting shelf-open ocean exchange near Cape Hatteras. The Gulf Stream actively exchanges water across the shelf edge of the SAB (Atkinson et al., 1983; Lee et al., 1991), influences the location and character of the Shelfbreak Jet detachment (Gawarkiewicz & Linder, 2006), and correlates with the alongshore transport convergence (Savidge & Bane, 2001).

The narrow band of ocean between the Gulf Stream and the continental shelf north of Cape Hatteras has been named the Slope Sea. The upper Slope Sea is occupied by the slope water, the exported shelf water, and intruded Gulf Stream water from rings and filaments (Csanady & Hamilton, 1988). The Gulf Stream can affect the shelf and Slope Sea circulations, as its relatively steep sea surface slope can penetrate the pressure field to the adjacent Slope Sea and the shelf (Xu & Oey, 2011). However, the processes and dynamics governing this complex circulation near Cape Hatteras remain poorly understood.

In this paper, currents on the shelf and the upper continental slope off Cape Hatteras are documented based on continuous 18-month time series of currents measured with moored instrumentation during PEACH. Building on earlier studies, these observations further reveal the mean circulation near Cape Hatteras and the character and predominant driving processes of its variability.

## 2. Data and Methods

In this study, we use observations from the PEACH field program, which employed a wide range of observing platforms over 18 months (April 2017–November 2018; Seim et al., 2022). We examine current velocities from bottom moored acoustic Doppler current profilers (ADCPs), temperature and salinity from CTDs, wind measurements from meteorological buoys, surface current velocities from High Frequency Radars, acoustic travel time from bottom-moored current and pressure-sensor equipped inverted echo sounders (CPIESs), and Sea Surface Temperature (SST) and Sea Surface Height (SSH) measured from satellites.

### 2.1. ADCP Data

Time-series of velocity profiles from the bottom to near the surface were collected using upward-looking Teledyne RDI ADCPs mounted on bottom moorings on the shelf and the upper continental slope, with vertical resolutions of 1 and 4 m, respectively. Processing and quality control of these data are detailed in Haines, Muglia, Bahr, et al. (2022). The moorings were placed along three isobaths: shelf moorings (600 kHz) along the 30-m isobath (B1, A4, A7, and B2), shelfbreak moorings (300 kHz) along the 100-m isobath north of The Point (A1, A2, and A3) and along the 250-m isobath south of The Point (A6 and A8) (Figure 1a). The along-shelf direction is defined as the orientation of the major principal axis of the depth-averaged velocity, while the cross-shelf direction is orthogonal to that (described further below). As the major principal axis directions are roughly parallel to the local isobaths, the term “along-isobath” is also used at the shelfbreak moorings. The positive along-shelf (along-isobath) direction is poleward, and the positive cross-shelf (cross-isobath) direction is offshore. Each ADCP was equipped with a temperature sensor, and in addition bottom temperature measurements from CTDs are available at several of the moorings (see below).

### 2.2. CTD Data

Bottom temperature and salinity were collected by the CTDs mounted on 2 shelf moorings (B1 and B2) and 3 shelfbreak moorings (A1, A2, and A8) (Haines, Muglia, Bahr, et al., 2022). At B1 and B2, two additional CTDs were placed near-surface (5 m) and mid-depth (15 m) to provide continuous observations of the water characteristics on the MAB and SAB shelves. Bottom temperature and pressure were available from CTDs at A4 and A7 shelf moorings, but the Conductivity sensors were corrupted and did not return useable data.

### 2.3. Wind Stress

We use meteorological data from two National Data Buoy Center (NDBC) buoys (44014 and 41025) and two PEACH buoys (B1 and B2). Wind speed and direction were directly measured by the buoys. The wind stress was computed from Coupled Ocean-Atmosphere Response Experiment (COARE) bulk flux algorithm, version 3.6 (Edson et al., 2013; Fairall et al., 2003). Wind stress values at a height of 10 m above the sea surface from European Center for Medium-Range Weather Forecasts Reanalysis v5 (ERA5; Hersbach et al., 2018) are also used in this study.

#### 2.4. HF Radar Data

The surface current velocities are a combined product derived from eight high frequency (HF) radars (4 CODAR and 4 WERA). Both types produced estimates of radial velocities on polar grids centered on each installation site but at differing resolution, with the WERA systems (relative to the CODAR systems) on a finer spatial resolution (1 vs. 6 km radially and 1° vs. 5° azimuthally) and temporal resolution (20 min vs. 1 hr). For this study, a combined product was formed from the two systems. WERA data were first quality controlled using the method of Mantovanni et al. (2012), then time-averaged to hourly intervals. The CODAR radial data were processed and quality-controlled following Haines et al. (2017). These radial velocities were then combined where the coverage grids overlap to produce estimates of the full current vector, on a pre-defined Cartesian spatial grid with a final grid resolution of 6 km and for each 1 hr. Experimentation using the native spatial sampling of radial velocity for both systems within an un-weighted least squares (UWLS) scheme (hfrprogs v2.1.2, downloaded from: <https://github.com/rowg/hfrprogs>) led to a decision to vector average (range and direction) the higher-resolution WERA radial data to the CODAR resolution (i.e., 6 km range and 5° radials) before combining to produce a product. A minimum of three radials from two sites within a 10 km radius were required for each solution. Two additional constraints were applied for each grid point. First, totals were removed when the root-mean square difference between the actual radial currents and the predicted radial currents from UWLS fit exceeded 0.3 m s<sup>-1</sup>. Second, uncertainty due to geometric dilution of precision was used to eliminate totals when a set of radials had limited angle coverage. The norm of the 2 × 2 covariance matrix between radial uncertainties as a measure of total uncertainty was computed using all angles and assuming each radial has an uncertainty of 1. Totals with this total uncertainty more than 1.25 cm s<sup>-1</sup> were removed.

Then the total velocity was despiked at each grid point by removing the consecutive data points separated by more than 0.5 m s<sup>-1</sup>. Outliers over three standard deviations (STD) from a running 7-day mean or more than 3.5 STD from the total mean were removed, following Archer et al. (2017). In addition, the grid points with data coverage over the 18 months lower than 40% were also removed. The quality controlled total velocity was further time-averaged to daily intervals.

#### 2.5. Gulf Stream Position Proxy

Variability in the Gulf Stream was inferred by three CPIESs (P5, P6, and P7) along the continental slope offshore of the SAB in water depth of about 1,300 m, roughly along the Gulf Stream average core position (25 cm SSH contour; Andres, 2021; Figure 1a). We use the hourly acoustic travel times ( $\tau$ ) measured at these sites (Andres, 2021) as the Gulf Stream position proxies in this study. The CPIESs' hourly  $\tau$  measurements are further 40-hr low-pass filtered. For a fixed transport, when the Gulf Stream moves onshore,  $\tau$  decreases. When the Gulf Stream moves offshore,  $\tau$  increases. This onshore/offshore motion of the Gulf Stream is associated with the passage of wave-like Gulf Stream meanders that move downstream past Cape Hatteras at about 40–55 km day<sup>-1</sup> (e.g., Savidge, 2004). Details of processing  $\tau$  are described in a technical report (Andres, 2020) and the Gulf Stream variability during PEACH is described in Andres (2021).

#### 2.6. Complex Empirical Orthogonal Function Analysis

A complex empirical orthogonal function (complex EOF) analysis was used to decompose the ADCP (hourly) velocity data into representative modes. Here it was applied to the complex time series  $\psi(x, t) = u(x, t) + iv(x, t)$ , where  $u$  and  $v$  represent the eastward and northward components of velocity, respectively. This method provides a description of the spatial variability of the velocity field EOFs, as well as the temporal variability of each independent EOF (principal component, or PC) by solving the eigenvalue problem for the complex covariance matrix (Edwards & Seim, 2008; Kaihatu et al., 1998). The resulting EOFs and PCs are vectors with a magnitude and a phase. To interpret the modes in a physical manner, each PC is rotated to the direction in which it has the most variance, and then the EOF is rotated accordingly. We reconstruct each mode by multiplying the eigenvectors with the PC,  $U_{\text{reconst}}(k) = e(k) \times PC(k)$ , for the  $k$ th mode, where  $e$  denotes the eigenvectors.

The confidence intervals of the variances explained by the different modes are given by the rule of thumb of North et al. (1982) as  $\Delta\lambda_k \approx \lambda_k \sqrt{2/N^*}$ , where  $\lambda_k$  is the explained variance of the  $k$ th mode and  $N^*$  is the degrees of freedom (DOF). Since the consecutive data values in a time series may not be independent, here we estimate the effective number of DOF, based on the integral time scale of the autocovariance function following Thomson



**Table 1**  
Summary of Annual Harmonic Analysis of the Depth-Averaged Velocity, and Mean Velocities, at the Moorings

| Moorings | Water depth (m) | Major axis (cm s <sup>-1</sup> ) | Minor axis (cm s <sup>-1</sup> ) | Orientation (°) | Phase (°)     | Mean velocity (cm s <sup>-1</sup> ) |             |
|----------|-----------------|----------------------------------|----------------------------------|-----------------|---------------|-------------------------------------|-------------|
|          |                 |                                  |                                  |                 |               | Along-shelf                         | Cross-shelf |
| B1       | 36              | 3.7 ± 2.2                        | 0.9 ± 0.7                        | 71.6 ± 14.9     | 191.5 ± 34.5  | -4.7                                | -0.8        |
| A4       | 30              | 3.6 ± 3.1                        | 0.0 ± 0.4                        | 96.7 ± 7.0      | 196.2 ± 47.2  | 2.8                                 | 4.3         |
| A7       | 30              | 3.7 ± 0.5                        | -0.4 ± 0.8                       | 20.1 ± 12.4     | 163.0 ± 8.0   | 6.0                                 | -1.4        |
| B2       | 30              | 4.1 ± 0.8                        | 0.1 ± 1.2                        | 33.4 ± 15.4     | 130.9 ± 11.5  | 9.0                                 | -1.0        |
| A1       | 99              | 2.0 ± 3.2                        | 1.3 ± 0.6                        | 100.8 ± 100.3   | 246.6 ± 150.2 | -5.0                                | 1.1         |
| A2       | 95              | 3.5 ± 2.5                        | 0.5 ± 0.9                        | 69.5 ± 17.2     | 222.5 ± 40.4  | -4.5                                | 0.8         |
| A3       | 98              | 3.0 ± 2.9                        | -1.5 ± 0.9                       | 73.2 ± 44.5     | 294.0 ± 77.0  | 9.0                                 | 9.0         |
| A6       | 236             | 5.3 ± 3.5                        | -0.3 ± 3.2                       | 47.1 ± 35.9     | 204.0 ± 36.9  | 55.2                                | -3.3        |
| A8       | 230             | 5.1 ± 2.9                        | 0.3 ± 2.4                        | 49.5 ± 27.9     | 207.7 ± 30.9  | 38.6                                | -0.9        |

*Note.* Orientation is counterclockwise relative to true east and phase is zero on 1 January. Error bars are 95% confidence intervals.

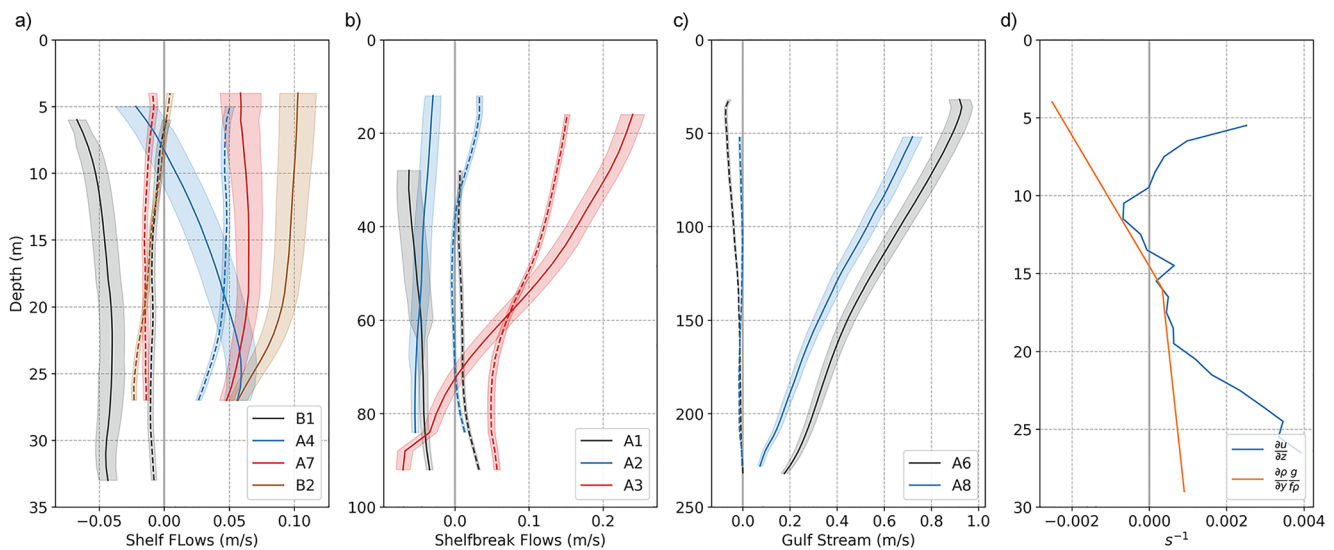
and Emery (2014). The hourly current velocities have an integral timescale of 1–2 days, resulting in an effective DOF value for the time series ranging from 195 to 270 by station, with a mean of 250. The same effective DOF is also used to compute the standard error and the correlation.

### 3. Results

#### 3.1. Mean Flows

We first examine the deployment-long average conditions, considering both the mass field and circulation. The continental shelf off Cape Hatteras is typically occupied by two distinct water masses: the relatively cold and fresh MAB shelf water and the warm and salty SAB shelf water (Figures 1a and 1b). The average along-shelf temperature difference between the B1 and B2 moorings, which are roughly 70 km north and southwest of Diamond Shoals respectively, ranges from 5°C at the surface to 10°C at the bottom, while the salinity difference is over 2 (Figure 1b). The MAB and SAB shelf waters each flow generally toward Cape Hatteras, which leads to a prominent convergent feature (Figure 1a). On the shelf between B1 and B2, the mean along-shelf velocity convergence is about  $1.1 \times 10^{-6} \text{ s}^{-1}$ , with the strongest convergence between B1 and A4. From north to south, the depth-averaged along-shelf mean flows are 4.7 cm s<sup>-1</sup> equatorward at B1, 2.8, 6.0, and 9.0 cm s<sup>-1</sup> poleward at A4, A7, and B2, respectively, which are the same order reported in earlier studies (Table 1; Savidge & Bane, 2001; Lentz, 2008a). The along-shelf mean velocity at B1 is relatively uniform in the vertical. The vertical shears of the mean along-shelf velocities at A7 and B2 increase with depth, most likely due to bottom friction. However, the vertical shear of the along-shelf velocity at A4 is large through the entire water column, with a magnitude of  $3.5 \times 10^{-3} \text{ s}^{-1}$  roughly the same as that at the bottom layer (below 20 m) at B2. The surface along-shelf velocity at A4 is equatorward like the MAB flow, but the bottom along-shelf velocity is poleward with the same magnitude as at B2, suggesting that it is a continuation of poleward SAB flow (Figure 2a).

The cross-shelf components of the mean flow are near zero but slightly onshore at most of the shelf moorings, except for A4 (Figures 1a and 2a). A 4.3 cm s<sup>-1</sup> offshore flow is observed at A4, suggesting that A4 is a favorable location for shelf water export in this region. The vertical shear of the cross-shelf flow at A4 shows a three-layer structure (Figure 2d). To assess whether the vertical shear reflects a thermal wind balance throughout the water column, we evaluate the terms of the thermal wind balance, using the density difference between B1 and B2 to estimate the along-shelf component of the density gradient ( $\partial\rho/\partial y$ ). Since the water temperature measured at A4 mostly resembles that at B1, while the temperature at A7 resembles that at B2, here  $\partial y$  is estimated as the along-shelf distance between A4 and A7. In the middle layer, between 10 and 20 m depth, the vertical shear and the density gradient terms roughly balance each other, and both change from negative to positive at about 15 m (Figure 2d). Friction from wind stress at the surface and bottom stress below likely explain the departure from the thermal wind balance in the surface and bottom layers.



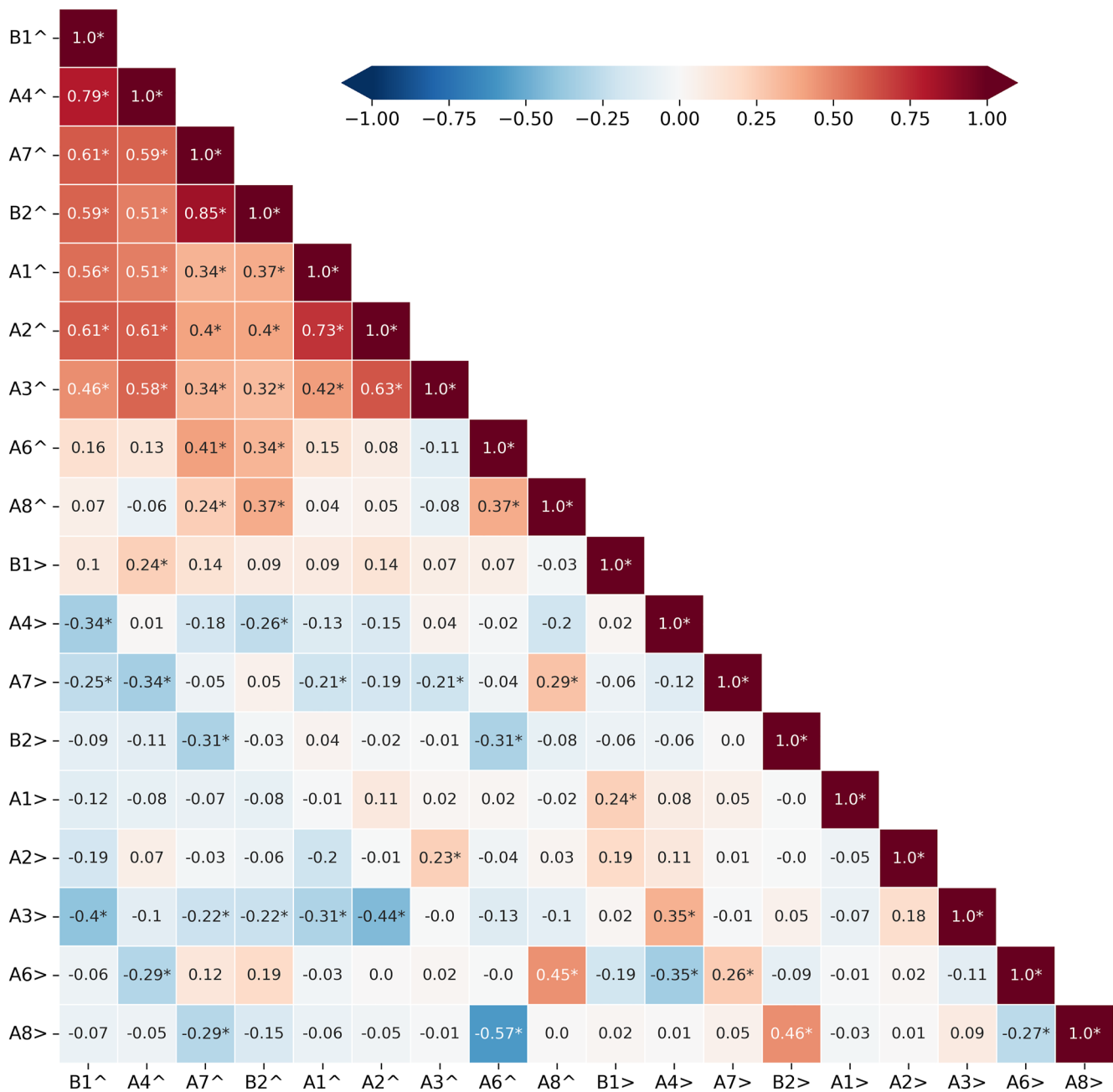
**Figure 2.** The mean profiles of the along-shelf (positive poleward) and cross-shelf (positive offshore) velocity at the (a) shelf, (b) northern shelfbreak and (c) southern shelfbreak (adjacent to the Gulf Stream) moorings. The solid curves are along-shelf velocity, and the dashed curves are cross-shelf velocity. The shadings are standard errors. (d) Terms in the thermal wind balance: the blue line for the vertical shear of the cross-shelf velocity term at A4 and orange line for the along-shelf density gradient term between B1 and B2.

Like the shelf flows, the flows at the upper slope are also convergent, with a mean along-shelf convergence of  $2.5 \times 10^{-6} \text{ s}^{-1}$  and a mean offshore flow at A3. At A1 and A2, the depth-averaged current velocities are  $5.1$  and  $4.6 \text{ cm s}^{-1}$  equatorward along the  $100 \text{ m}$  isobath, respectively, while at A3 it is  $12.9 \text{ cm s}^{-1}$  toward  $60^\circ$  clockwise from the true north (Figure 1), indicating the Gulf Stream's influence. A8 and A6 are each located within the shoreward flank of the mean Gulf Stream ( $\sim 10 \text{ km}$  inshore of the  $25\text{-cm}$  mean SSH contour), where the depth-averaged velocity is  $38.7 \text{ cm s}^{-1}$  at A8 and  $55.2 \text{ cm s}^{-1}$  at A6. The along-isobath direction at these two moorings is the same as the along-stream direction. The vertical shear of the mean along-stream flow at A6 and A8 is  $4 \times 10^{-3} \text{ s}^{-1}$ , but the flow is overall stronger at A6 (Figure 2c). As the Gulf Stream approaches Cape Hatteras, the bathymetry of the continental slope steepens and the lateral amplitude of Gulf Stream meanders typically decays (Andres, 2021; Savidge, 2004). The smaller path variance envelope suggests that the Gulf Stream would not wander laterally away from A6 as much as it would from A8, and the weaker reverse flow caused by decaying frontal eddies at A6 may also explain the faster mean current speed there compared to A8. Strong vertical shear of the along-shelf flow is also observed at A3 (Figure 2b). At A3, the mean along-shelf velocity is only  $1/4$  of that at A6, but they have approximately the same vertical shear, which may be due to the Gulf Stream often overlying A3.

The depth-averaged mean flows at the three northern shelfbreak moorings all have an offshore component:  $0.8 \text{ cm s}^{-1}$  at A1,  $1.5 \text{ cm s}^{-1}$  at A2, and  $11.3 \text{ cm s}^{-1}$  at A3. The cross-shelf velocities all have a similar vertical structure, with the largest velocity near the surface, first decreasing with depth and then increasing (Figure 2b), which is consistent with Lentz (2008b) although with an additional depth-independent offset that results in offshore flow at all depths. At A6 and A8, the cross-shelf flow is on-shore at speeds of  $3$  and  $1 \text{ cm s}^{-1}$ , respectively (Figures 1a and 2c). On average, along the shelfbreak off Cape Hatteras, the open-ocean (Gulf Stream) water intrudes onto the shelf at and south of A6, while the shelf water exports to the open ocean north of the Point.

### 3.2. Variability of the Depth-Averaged Velocity

At all 9 moorings, most of the variance is along the local isobath (1 standard deviation ellipses in Figure 1a). The 40-hr low-pass filter removes the tidal signal in the current velocities and decreases the total variance by 3%–22%, mostly in the cross-shelf/cross-isobath direction. With the exception of the two Gulf Stream moorings (A6 and A8), A4 shows the highest standard deviation of depth-averaged velocity, consistent with a back-and-forth passage of the Hatteras Front over A4. The center of each standard deviation ellipse is plotted at the tip of a mean flow vector, which shows that about 66.7% of the time the entire velocity vector at each mooring is located within



**Figure 3.** Correlation map between along-shelf and cross-shelf velocities at the moorings. <sup>^</sup> stands for along-shelf velocity and <sup>></sup> for cross-shelf velocity. \* marks where the result is statistically significant ( $p$  value  $\leq 0.001$ ).

the ellipse. At the four shelf moorings, the chance of having an equatorward flow decreases from north to south. The occurrence of an equatorward flow at A6 is less likely than at A8. Since A6 is closer to the Point and the lateral amplitudes of Gulf Stream meanders typically become smaller as the meanders propagate northeastward (Andres, 2021; Savidge, 2004), this results in smaller (and perhaps fewer) frontal eddies passing by to generate reverse (southwestward) flow. Most of the time, the flows at A4 and A3 have an offshore component, which further suggests that A4 and A3 are favorable locations for shelf water export.

Temporal correlations between elements of the mooring array are quite variable. At three pairs of moorings, the along-shelf velocities are highly correlated, with a correlation higher than 0.7 (Figure 3). They are the two MAB shelf moorings (B1 and A4), the two SAB shelf moorings (A7 and B2), and the two northern-most shelfbreak

moorings (A1 and A2). A3 is influenced by both the Shelfbreak Jet and the Gulf Stream. Furthermore, the along-shelf velocities at the MAB shelf moorings are well correlated with those at the SAB shelf moorings (correlation  $>0.5$ ). Along-shelf transport on the continental shelf is typically correlated with along-shelf winds, here at Cape Hatteras as elsewhere (shown below, and as in Savidge & Bane, (2001)). In addition, all the measured along-shelf velocities north of Cape Hatteras (B1, A4, A1, A2, A3) are well correlated. South of Cape Hatteras, the correlations between the along-shelf velocities at the shelf moorings (A7 and B2) and the shelfbreak moorings (A6 and A8) are much smaller. The low correlation between the two Gulf Stream measurements (at A6 and A8) is due to propagating Gulf Stream meanders. To address the time lag between these two time series, lagged correlation analysis is applied to the depth-averaged along-shelf velocity at the two moorings. They reach their maximum correlation of 0.83 at a time lag of 25 hr, with the velocity at A8 leading A6. In this region, Gulf Stream meanders have been observed to propagate downstream (northeastward) at speeds of 40–55 km day<sup>-1</sup> (Andres, 2021; Savidge, 2004). The distance between A6 and A8 is about 54 km. Thus, the time that it takes for Gulf Stream meanders to propagate from A6 to A8 is roughly a day, which agrees with the time lag of the maximum correlation.

In general, cross-shelf velocities are less correlated than along-shelf velocities. Some relatively high negative correlations exist between the cross-shelf velocity at one mooring and the along-shelf velocity at the northern adjacent mooring, suggesting that a stronger equatorward flow from the north coincides with a stronger offshore flow. The positive correlation between the cross-shelf velocity at A2 and the along-shelf velocity at its southern neighbor A3 suggests that a stronger offshore flow accompanies a stronger poleward flow from the south. Together these highlight the converging nature of the flows in this region. The positive correlation between the cross-shelf velocity at A7 and the along-shelf velocity at A8 indicates that the cross-shelf velocity at A7 is offshore when the Gulf Stream moves onshore at A8. Another striking pattern in the correlation map is the positive correlation between the cross-shelf velocities at laterally adjacent moorings (e.g., B1 and A1, A4 and A3, A7 and A6, B2, and A8), possibly reflecting the shelf-open ocean water exchange. When open ocean water intrudes on the shelf, an onshore flow would be observed both at the shelfbreak and on the shelf. Likewise, an offshore flow would be observed when shelf water exports to the open ocean.

The depth-averaged current velocities at most sites are correlated with the wind except for those at A6 and A8 where the currents associated with the Gulf Stream dominate the flow. The along-shelf current velocities at all four shelf moorings have a correlation higher than 0.53 with the southward component of wind stress at NDBC buoy 44014 at time lags ranging from 7 to 10 hr. The high correlations resemble that between the along-shelf transport and the wind in Savidge and Bane (2001), suggesting the along-shelf current variability is mostly driven by the wind. The along-isobath velocities at the three northern shelfbreak moorings are also correlated ( $p$  value  $\leq 0.001$ ) with the wind stress, but the correlation is between 0.3 and 0.5, not as high as that on the shelf.

### 3.3. Annual Cycle

Annual variations of depth-average velocity, defined as a 12-month harmonic fit using UTide (Codiga, 2011), are consistent at all the moorings, with major axis amplitudes of 2–5.5 cm s<sup>-1</sup> (Table 1). These results are very similar to those from Lentz (2008b) for locations north of the PEACH moorings. The major axis amplitudes are significantly different from zero at the 95% confidence level at all the moorings except for A1. But at all the sites, the variance of the reconstructed annual velocity accounts for less than 2% of the total variance. Similar to the principal axes of the subtidal flow, the orientation of the annual variation is generally along isobath. At all the moorings except A4, the amplitude of the major axis of the annual variation is smaller than the mean along-isobath velocity, indicating the annual variation doesn't reverse the mean flow, but just modulates the magnitude at these moorings. The along-isobath flows are primarily in phase and experience the strongest equatorward modulation in the winter months (November–March), which corresponds with historical observations from the MAB and northern SAB (Lentz, 2008b; Savidge & Savidge, 2014). For example, the maximum equatorward along-shelf flow at B1 occurs in January, and the along-shelf flow is weakest, but still equatorward, in June. However, at A4, since the annual variation exceeds the mean along-shelf velocity, the flow is equatorward in the winter but poleward in the summer.



### 3.4. Vertical Variability of Currents

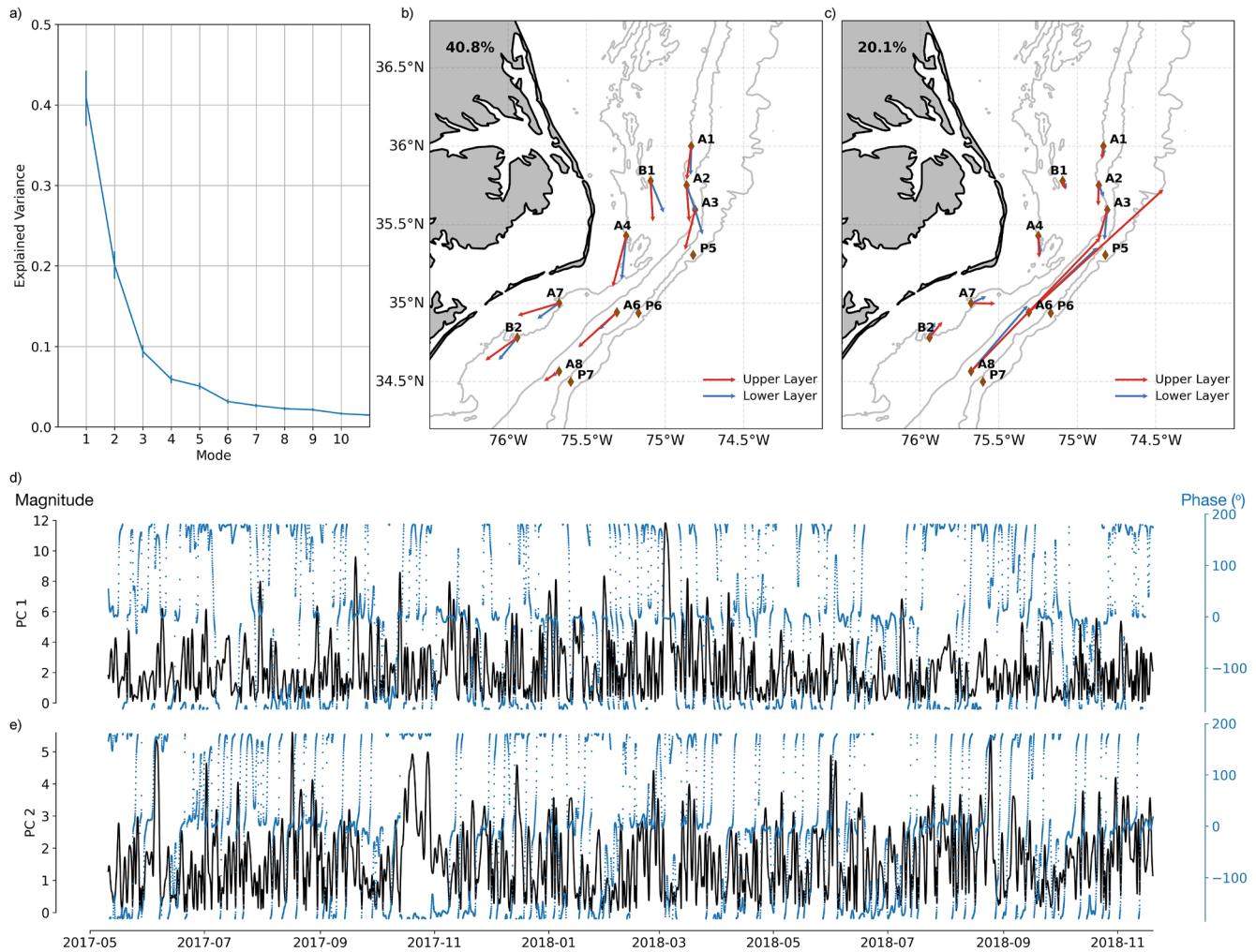
To determine whether a layered ocean would accurately represent the vertical structure of the horizontal currents, the complex EOF analysis was first applied to the 40-hr low passed current profiles through the full water column at each of the 9 moorings individually. At each individual mooring, the first two modes explain more than 90% of the total variance, a reasonable threshold for truncating an EOF expansion (Venegas, 2001). An along-shelf, nearly depth-uniform vertical structure of the first EOF mode is evident at each mooring, with reductions in amplitude toward the bottom and a counter-clockwise veering of the currents with depth. The second EOF mode is characterized by opposite flowing currents at the surface and bottom layers, with a zero crossing at mid depth. Therefore, a two-layer current structure should be sufficient to address these vertical variations. In this study, the upper and lower 1/3 of the water column are used to represent the upper and lower layers representatively.

### 3.5. Array-Wide Spatial Variability

To characterize the array-wide spatial variability of the flows off Cape Hatteras, a complex EOF analysis was applied to the velocity averaged over the upper and lower 1/3 of the water column at all 9 moorings. Since the velocity at A6 is highly correlated with that at A8 with a correlation of 0.83 at 25-hr lag and the complex EOF method (used with vector inputs) is limited in its ability to resolve propagating features, we lagged the velocities at A8 by 25 hr to account for the effect of the downstream propagating Gulf Stream wave-like meanders that move from A8 to A6. All the input current time series were 40 hr low-pass filtered with the temporal mean removed. The modes are found to be well separated (Figure 4a). In this study, we will focus on the first two leading complex EOF modes, which together can explain 61% of the total variance. A sensitivity analysis suggests that the basic spatial structure of these two leading modes is robust regardless of different combinations of lags applied to the velocities at A6 and A8, discussed fully below.

The first mode, designated EOF-1, explains 40.8% of the total variance. EOF-1 shows an along-shelf flow pattern with codirectional eigenvectors at each mooring roughly aligned with the local isobath (Figure 4b). In this region, the along-shelf transport has been related to wind forcing (Savidge & Bane, 2001), and EOF-1 is likely the expression of the wind-driven flow during PEACH. At each mooring in water depth  $\leq 100$  m, the eigenvector in the lower layer is to the left of that in the upper layer, with reduced magnitude, possibly due to the effect of the bottom boundary layer. At A6 and A8, the eigenvector in the lower layer (deeper than 150 m) is nearly aligned with that in the upper layer but has larger magnitude reduction than is observed at the shallower sites. The phase of PC1 is mostly near 0 and  $\pm 180^\circ$  (Figure 4d), suggesting the first mode is more rectilinear than rotary, which is also consistent with a wind-driven effect. To examine if Mode 1 is wind-driven, the lagged complex correlations between PC1 and the wind stress at NDCB buoy 44014, B1, NDCB buoy 41025, and B2 were calculated. The results are summarized in Table 2. The maximum correlations were mostly found at a lag of  $-9$  to  $-7$  hr. The negative lag indicates that the wind stress is leading the along-shelf flow by  $\sim 8$  hr. Angular displacements (phases) of the complex correlation results between the wind stresses and PC1 are around  $-90^\circ$ . For the complex correlation analysis, the real component of PC1 is associated with the  $x$ -axis and the imaginary component with the  $y$ -axis. Since the real component of PC1 contains 97% of the total variance, PC1 is mostly along the  $x$ -axis with a phase of 0. The  $-90^\circ$  phase suggests that the southward wind elicits the strongest equatorward along-shelf flow in EOF-1. At B1, the correlation between the real component of PC1 and the southward wind stress is 0.68 at 8-hr lag. The same lagged complex correlation analysis was performed between PC1 and the ERA-5 reanalysis wind stress over the entire PEACH region (Figure 5). The wind stress over the southern MAB shelf has the highest correlation with PC1. Similar to the wind stress measured at the buoys, the southward component of the reanalysis wind stress drives the along-shelf flow and leads the flow by 8–12 hr.

To further explore the relationship between the along-shelf flow pattern and the wind, spectral analysis was applied to the real component of PC1 and the southward component of the wind stress at B1 (Figure 6), where the wind stress and PC1 has the highest correlation. The multitaper method (Percival & Walden, 1993) was used in order to preserve as much information as possible regarding the low frequency variability. The energy of PC1 and the wind stress in the weather band (2–10 days) is at a similar level (Figure 6a). However, the energy of PC1 is more concentrated within the intraseasonal band (about 10 days–3 months), while the wind has more energy within an even lower frequency band (longer than 3 months) (Figure 6a). This is consistent with the relatively weak annual variation of the velocity at all the moorings. The two time series are significantly coherent at most



**Figure 4.** (a) The percentage of variance explained by each empirical orthogonal function (EOF) mode and associated standard error, estimated after North et al. (1982). Spatial pattern of (b) Mode 1 (EOF-1: 40.8% variance explained) and (c) Mode 2 (EOF-2: 20.1% variance explained). Magnitude and phase of (d) PC1 and (e) PC2. The black line is magnitude and the blue dots are phase.

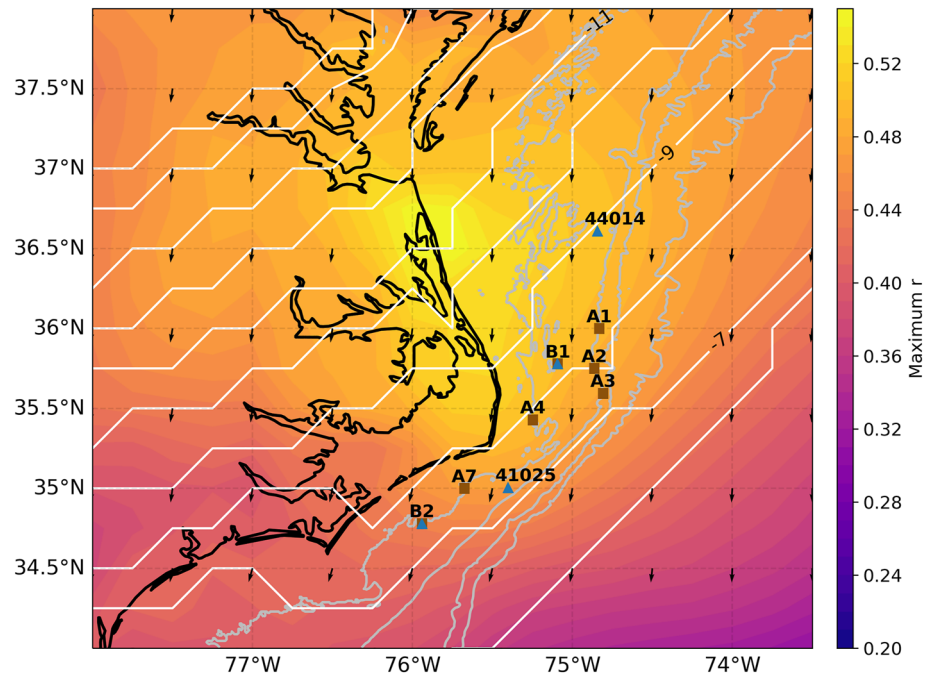
of the resolvable frequencies (Figure 6b). The 8-hr phase difference computed from the correlation analysis is mostly found at the weather band (Figure 6c).

To study the spatial structure of the wind-driven flow pattern, we created composite averaged maps of SST and surface currents measured with HF Radar when the daily averaged PC1 is over its 80th percentile (defined as positive PC1) and below its 20th percentile (defined as negative PC1) (Figure 7). When PC1 is identified as positive, the average wind stress at B1 is  $0.14 \text{ N m}^{-2}$  toward  $171^\circ$  clockwise from north and the shelf surface currents flow equatorward. The composite SST and surface current both indicate that the relatively cold MAB water converges with the warm SAB water south of Cape Hatteras (Figure 7b). The surface current map further suggests that the shelf water is exported along the edge of the Gulf Stream. When PC1 is identified as negative, the average wind stress at B1 is  $0.05 \text{ N m}^{-2}$  toward  $36^\circ$  clockwise from true north and the shelf currents reverse to flow poleward. Driven by the wind, the surface current velocity of the Gulf Stream

**Table 2**  
The Magnitude, Time Lag, and Phase of the Maximum Lagged Complex Correlation Between PC1 and the Wind Stress at 44014, B1, 41025, and B2

|       | Maximum $r$ | Lag (h) | Phase ( $^\circ$ ) |
|-------|-------------|---------|--------------------|
| 44014 | 0.50        | -9      | -88.9              |
| B1    | 0.53        | -8      | -89.0              |
| 41025 | 0.48        | -7      | -95.3              |
| B2*   | 0.48        | -9      | -102.8             |

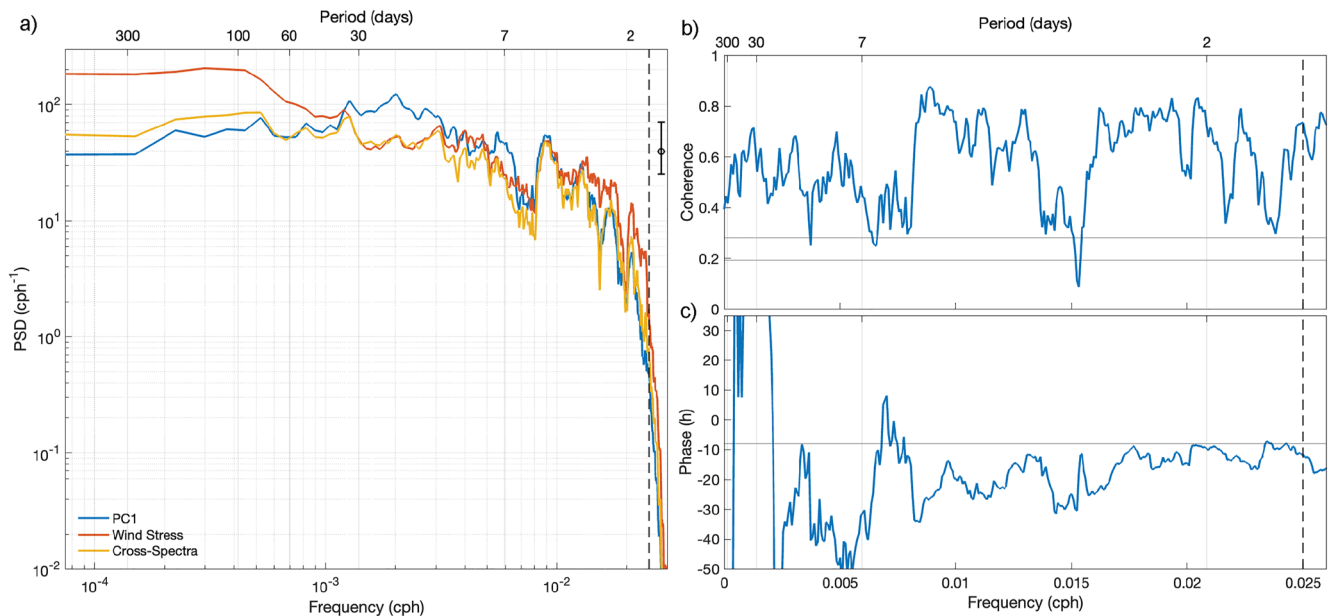
*Note.* All wind stress records have the same duration as the velocity data, except for B2. The wind stress record at B2 is about 16 months. The correlation is computed using the truncated 16-month PC1 and wind stress at B2, marked with \*. The locations of the buoys are shown in Figure 5.



**Figure 5.** The magnitude, time lag and phase map of the maximum lagged complex correlation between PC1 and the ERA-5 wind stress. The background color is the magnitude of maximum correlation. The white contours are the time lag. Negative time lag means that the wind stress is leading PC1. The black arrows show the phase of the complex correlation.

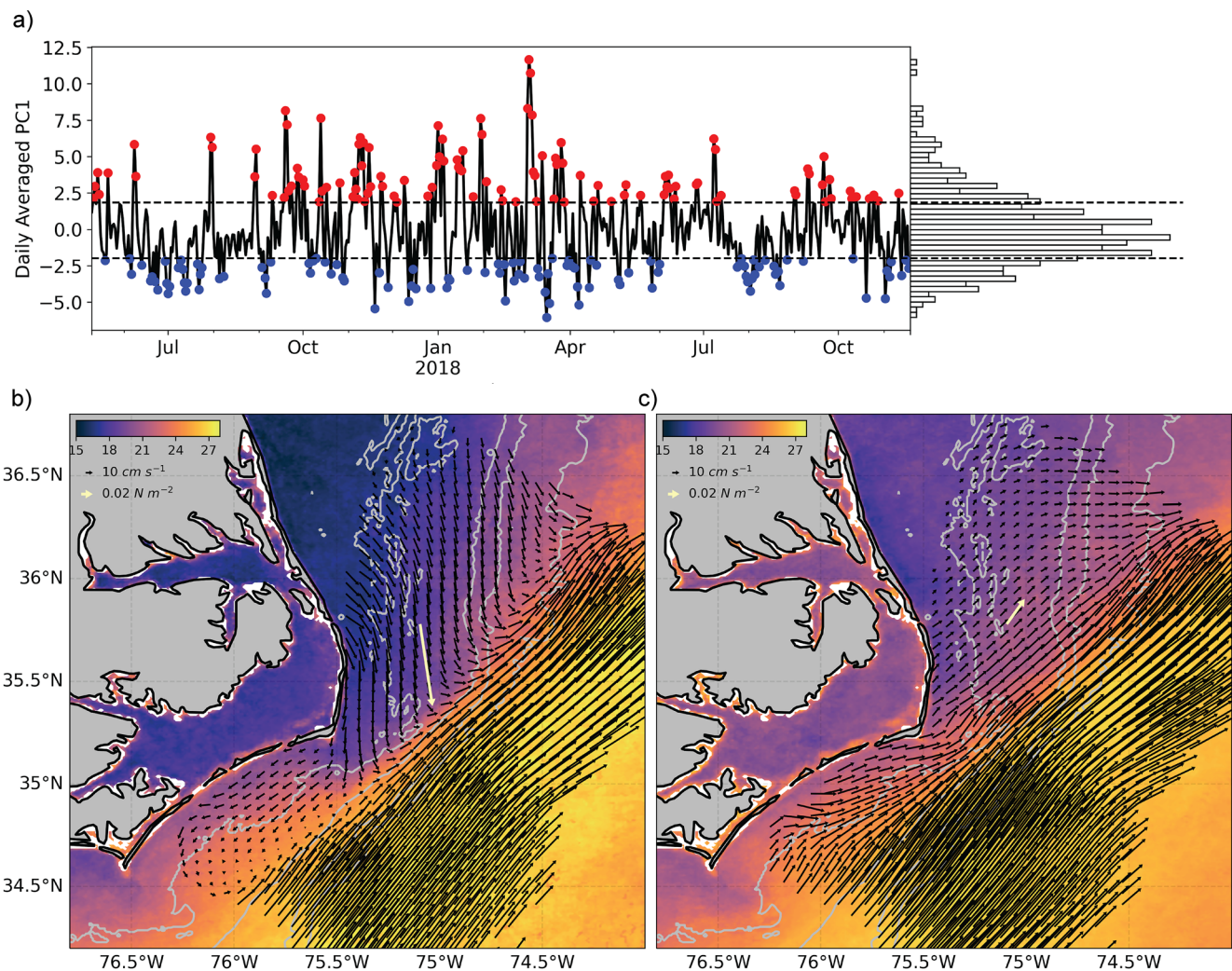
increases compared to that when PC1 is positive. The MAB water converges with the SAB water north of Cape Hatteras and the shelf water is exported to the Slope Sea (Figure 7c).

EOF-2 shows an along-shelf flow pattern that is converging toward Cape Hatteras, with the strongest convergence between A4 and A7 on the shelf and between A3 and A6 at the shelfbreak (Figure 4c). In contrast to the



**Figure 6.** (a) Auto- and cross-spectra of the real component of PC1 and the southward component of the wind stress at B1. (b) Coherence and (c) phase spectra between the two time series. The vertical dashed lines mark 1/40 cph, the cut-off frequency of the low-pass filter. The error bar in (a) is 95% confidence interval. The two horizontal lines in (b) are 95% (coherence = 0.19) and 99% (coherence = 0.28) confidence levels. The horizontal line in (c) marks -8 hr phase difference.

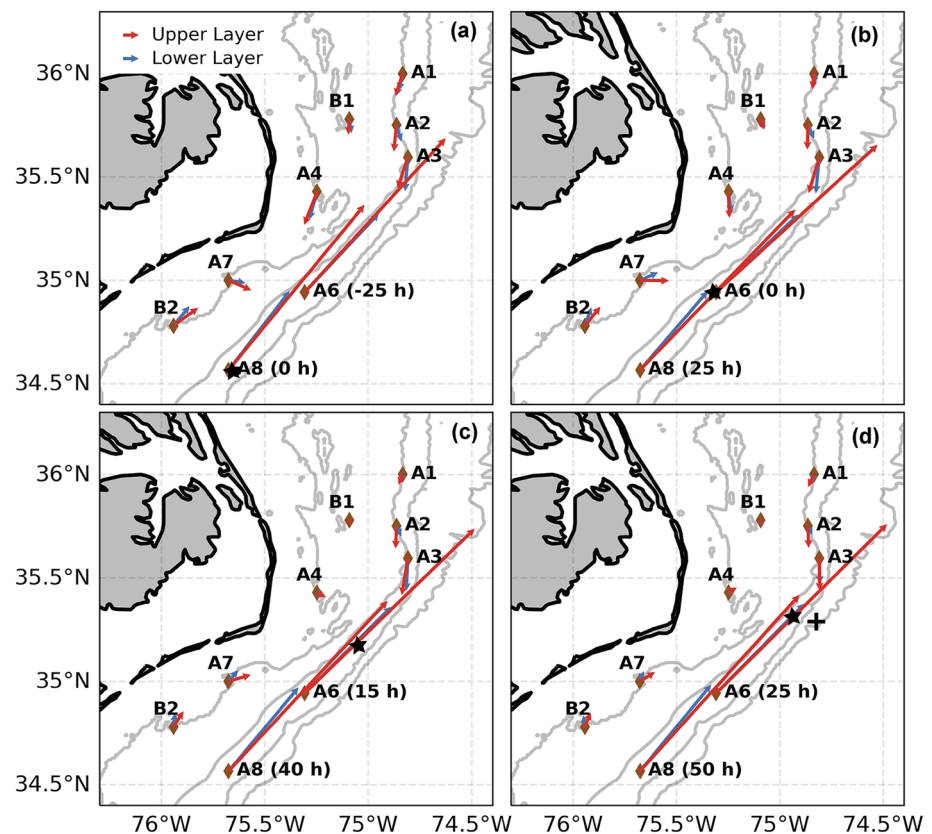




**Figure 7.** (a) Time series and histogram of the daily averaged real component of PC1. Two dashed lines are 20th and 80th percentile of PC1. Red/blue dots mark the days when PC1 is larger/smaller than its 80th/20th percentile. Averaged Sea Surface Temperature, high frequency radar measured surface current and the wind stress at B1 (yellow arrow) on the days when (b) PC1 is larger than its 80th percentile (positive PC1) and (c) PC1 is smaller than its 20th percentile (negative PC1).

converging pattern found in the mean flow field, the EOF-2 pattern displays a strong cross-shelf component at A7 rather than A4. We conducted a sensitivity test to explore how different lags applied to A6 and A8 prior to the EOF calculations influenced the position of alongshelf convergence and cross-shelf export (Figure 8). Since the positive lags represent downstream meander propagation, an increasing lag was applied to data from A6 and A8 prior to EOF decomposition to represent the Gulf Stream velocities at locations moving downstream from Raleigh Bay to The Point. Considering a propagation speed of 48 km/day, the 15-hr lagged velocity from A6 should resemble the Gulf Stream velocity about 30 km downstream and the 25-hr lagged velocity from A6 should resemble the Gulf Stream velocity about 50 km downstream, shown as the stars in Figure 8. The analysis shows that as the lag is increased, the strong cross-shelf component in EOF-2 is found further to the north and is eventually located north of Diamond Shoals for a lag of 15 hr applied to A6 and 40 hr to A8 (Figure 8). Like EOF-1, the EOF-2 eigenvector in the lower layer is to the left of that in the upper layer, but with larger reduction of the magnitude. The magnitudes of the eigenvectors at A6 and A8 significantly exceed those at the other moorings, which reflects the dependence of EOF-2's converging spatial pattern on the Gulf Stream. This is also demonstrated by the high correlation between PC2 and the Gulf Stream position proxies ( $r = -0.74$  with sound travel time ( $\tau$ ) at P7,  $r = -0.69$  at P6, and  $r = -0.42$  at P5; see Figure 1), which is consistent with strong Gulf Stream influence on along-shelf transport convergence (Savidge & Bane, 2001). When the Gulf Stream moves onshore, the convergence on the shelf becomes stronger. The phase of PC2 suggests that the second mode is also



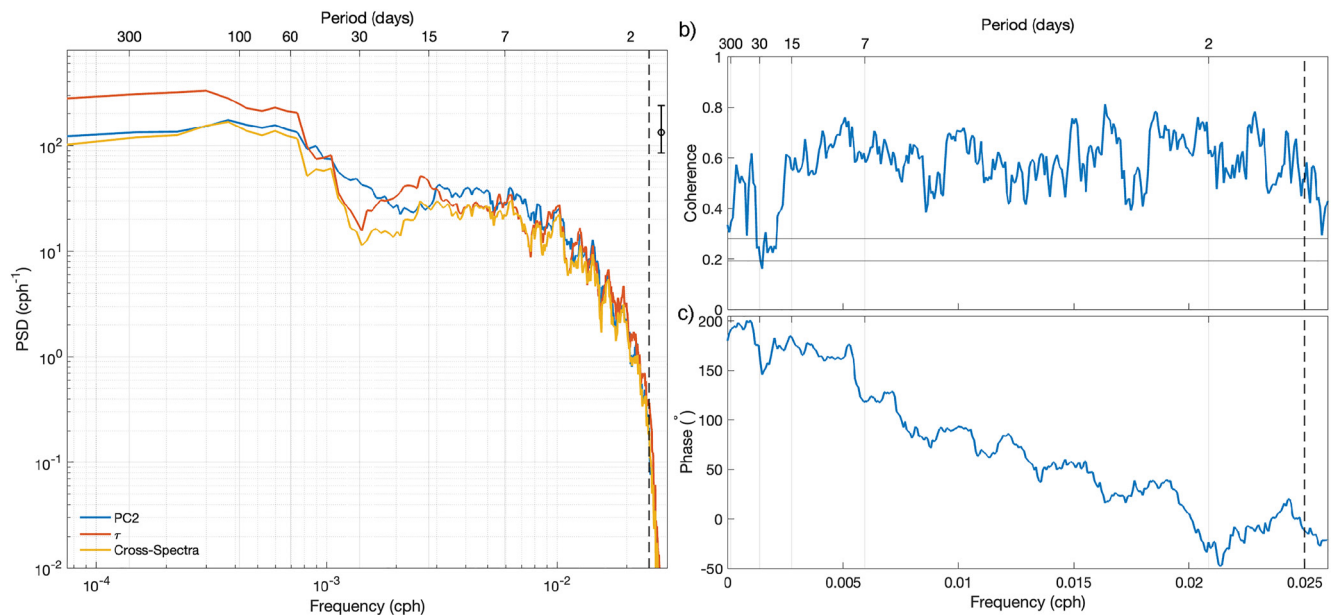


**Figure 8.** EOF-2 with different lags applied to the velocities at A6 and A8. The stars show the estimated location where the velocity resembles the lagged velocity. The cross (d) shows the location of the Gulf Stream position proxy in Savidge and Bane (2001).

more rectilinear than rotary and the variance of PC2 mostly lies in the real component (Figure 4e), which means the convergence in EOF-2 becomes stronger and weaker and even reverses to divergence at times, but not much rotation is involved.

Spectral analysis was applied to PC2's real component and  $\tau$  at P7 (Figure 9), where the correlation between  $\tau$  and PC2 is highest. In the 2–7-day band, all the peaks in the auto-spectrum of PC2 follow those of  $\tau$ . Their energies are both lower in the 15-day–1-month band and higher in the lower frequency band (longer than 40 days). The high-frequency signal in PC2 is likely related to the wave-like Gulf Stream meanders in the 2–15-day band, while the low-frequency signal might be driven by changes in Gulf Stream transport off Cape Hatteras (Andres, 2021) and lower-frequency lateral (onshore/offshore) shifts in the mean position of the Gulf Stream. PC2 is significantly coherent with  $\tau$  at nearly all frequencies (Figure 9b). Onshore movement of the Gulf Stream decreases the sound travel time at a CPIES but increases the flow convergence (PC2), which results in an inherent  $\pm 180$  phase difference between PC2 and  $\tau$ . Since the input velocity is lagged by 25 hr at A8 to eliminate the Gulf Stream meander propagation signature, the resulting PC2 resembles the Gulf Stream movement near A6. The positive phase difference between PC2 and  $\tau$  at P7 indicates that  $\tau$  is leading PC2 (Figure 9c). The converging pattern of EOF-2 is largely driven by the Gulf Stream meander process and due to the decreasing meander amplitude approaching The Point, the variance of  $\tau$  in the meander band (2–15 days) decreases from P7 to P5 (Andres, 2021). Together these factors may explain the weakening correlation between PC2 and  $\tau$  from P7 to P5 noted above.

Based on PC2, we created another set of composite maps of SST and surface currents from HF Radar under the same conditional averaging conventions as PC1 (Figure 10). When PC2 is identified as positive (over its 80th percentile), the SST, SSH (25-cm contour) and surface currents all suggest the Gulf Stream is in a more onshore position in Raleigh Bay (Figure 10b). The largest surface current convergence is south of Cape Hatteras, while the along-shelf SST gradient is the strongest north of Cape Hatteras. The shelf water is exported to the edge of the Gulf Stream south of Cape Hatteras, but to the Slope Sea north of Cape Hatteras. When PC2 is



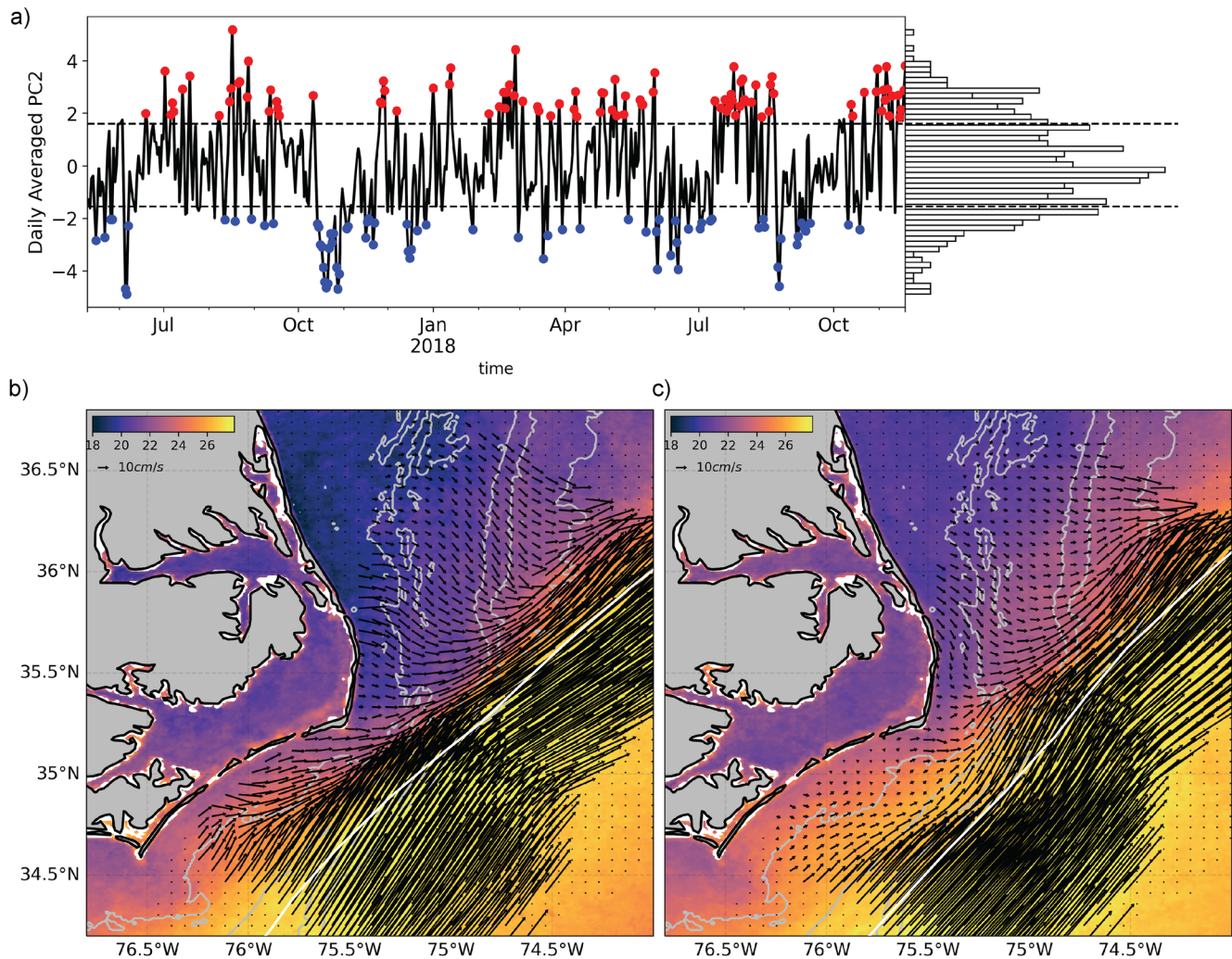
**Figure 9.** (a) Auto- and cross-spectra of the real component of PC2 and the sound travel time ( $\tau$ ) at P7. (b) Coherence and (c) phase difference between PC2 and  $\tau$  at P7. The vertical dashed lines mark 1/40 cph, the cut-off frequency of the low-pass filter. The error bar in (a) is 95% confidence interval. The two horizontal lines in (b) are 95% and 99% confidence levels.

identified as negative (below its 20th percentile), the Gulf Stream is positioned more offshore in Raleigh Bay (Figure 10c). The shelf water converges and is exported to the Slope Sea north of Cape Hatteras. The cold MAB water is constrained further inshore compared to that under the positive PC2 condition. The positive ( $\geq 80$ th percentile) and negative ( $\leq 20$ th percentile) PC2s used in the composite maps are at local maxima and minima, which mostly capture the crest and the trough of each passing Gulf Stream meander. A crest/trough-shaped Gulf Stream appears in the conditionally averaged SST and surface currents but not in the SSH, since the short wavelengths ( $\sim 180\text{--}380$  km) and fast propagation speeds ( $\sim 40\text{--}55$  km/day) of Gulf Stream meanders (Andres, 2021; Savidge, 2004) relative to the spacing of SSH overpasses ( $\sim 300$  km) and the repeat interval in time (10 days), leave the meanders poorly represented in the SSH record.

### 3.6. Combined Effects of Wind and Gulf Stream

To examine the combined effects of the wind and the Gulf Stream, we further conditionally average the SST, surface velocity within the PEACH domain, and the depth-averaged velocity at the moorings under the following four conditions: (a) PC1 and PC2 are both positive, (b) PC1 is positive and PC2 is negative, (c) PC1 is negative and PC2 is positive, and (d) PC1 and PC2 are both negative (Figure 11). In all the conditions, the averaged reconstructed velocity field from the first two EOF modes, plus the mean flow field, is nearly indistinguishable from (not statistically different from) the total velocity of the upper and lower layers at all the moorings, which further supports the hypothesis that the Gulf Stream and the wind are the primary drivers of the complex flow patterns around Cape Hatteras. The four conditions have about equal occurrence percentages of 20%–28%, but the temperature variations between them correspond to the time of year when each is most prevalent. The MAB shelf and Pamlico Sound have the coldest average SST in condition 1, and the warmest in condition 3, owing to the fact that condition 1 occurs more often in the winter and condition 3 more in the summer. Conditions 2 and 4 are more evenly distributed throughout the year.

- In condition 1 (positive PC1 and positive PC2), the stronger equatorward flows caused by the wind coupled with the enhanced convergence due to the onshore movement of the Gulf Stream produce increased MAB shelf flow, a strong Shelfbreak Jet reaching the southernmost extent to The Point, and little to no flow on the SAB shelf. Strong convergence occurs at the edge of the Gulf Stream where the MAB water flows into the Gulf Stream. One extreme case in this condition is the shelf water cascading event documented by Han

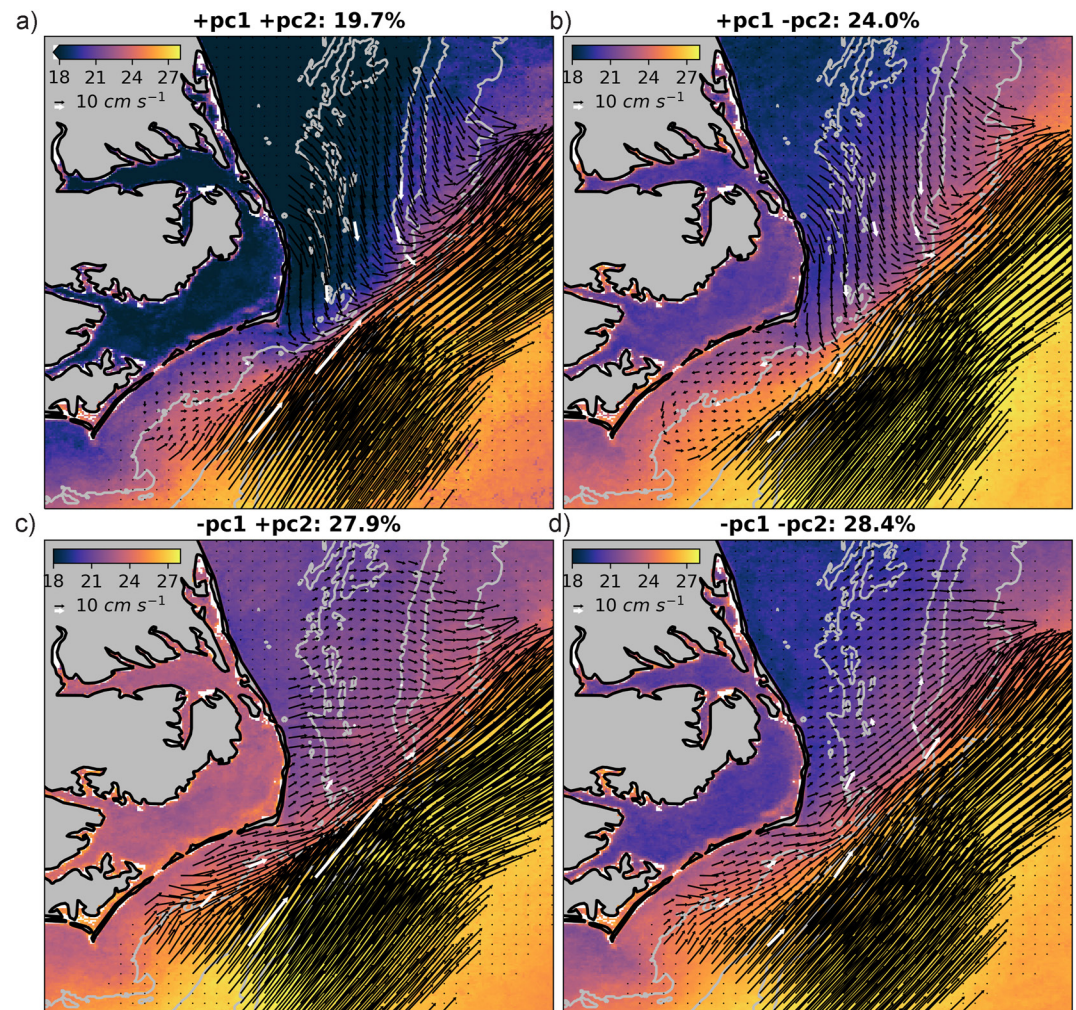


**Figure 10.** (a) Time series and histogram of the daily averaged real component of PC2. Two dashed lines are 20th and 80th percentile of PC2. Red/blue dots mark the days when PC2 is larger/smaller than its 80th/20th percentile. Averaged Sea Surface Temperature, high frequency radar measured surface current, 25-cm contour of Sea Surface Height (white contour) on the days when (b) PC2 is larger than its 80th percentile (positive PC2) and (c) PC2 is smaller than its 20th percentile (negative PC2).

et al. (2021). The shelf water became denser than the Gulf Stream water due to strong cooling after a winter storm and then cascaded beneath the Gulf Stream driven by the density gradient.

- In condition 2 (positive PC1 and negative PC2), the flow speeds at A6 and A8 are much reduced, consistent with the offshore position of the Gulf Stream. The Shelfbreak Jet is still present but weakened by the divergence caused by the offshore movement of the Gulf Stream. The wind-driven equatorward flows and the Gulf Stream-driven divergence lead to a “mustache feature” at Cape Hatteras, where the MAB water on the inner shelf flows past the cape onto the SAB shelf and the MAB water on the outer shelf turns and flows northeastward with the Gulf Stream and exports to the open ocean (cf., Seim et al., 2022).
- In condition 3 (negative PC1 and positive PC2), the wind-driven poleward flows and the Gulf Stream-driven convergence result in near zero along-shelf flows north of Cape Hatteras and a strong poleward SAB flow, with the largest along-shelf convergence between A4 and A7. The depth-averaged currents at the two northernmost shelfbreak moorings A1 and A2 are also near zero. The along-isobath component of the surface currents from the HF-Radar data north of Cape Hatteras both on the shelf and at the shelfbreak is near zero as well. However, the surface currents show a pronounced offshore component.
- In condition 4 (negative PC1 and negative PC2), as a result of the wind-driven poleward flows and the Gulf Stream-driven divergence, both the MAB flow and the Shelfbreak Jet are reversed, flowing poleward. The





**Figure 11.** Averaged Sea Surface Temperature, high frequency radar measured surface current (black arrows) and the depth averaged velocity at the moorings (white arrows) on days when (a)  $PC1 > 0$  and  $PC2 > 0$ , (b)  $PC1 > 0$  and  $PC2 < 0$ , (c)  $PC1 < 0$  and  $PC2 > 0$ , and (d)  $PC1 < 0$  and  $PC2 < 0$ . The percent occurrence of each condition is included in the subpanel title.

SAB flow is poleward, similar to that in condition 3 but weaker. The surface currents also have an offshore component that doesn't exist in the depth-averaged currents.

#### 4. Discussion

The 18-month observations of current velocity off Cape Hatteras confirm a convergent mean circulation pattern on the shelf and upper continental slope. The bottom-mounted ADCPs deployed during PEACH provided continuous observations of the current velocity profiles not available from pointwise current meter moorings in prior studies. The mean depth-averaged along-shelf currents are convergent between any adjacent pairs of shelf moorings, with the strongest convergence between A4 and B1. The strongest surface convergence is found south of A4 and the strongest bottom convergence is found north of A4. This suggests that, in the mean flow field, the baroclinic Hatteras Front is right above A4, with the zero isotach deepening toward the north. The mean SST pattern shows that the largest surface temperature gradient is roughly between A4 and A7, closer to A4. The temporal mean of the depth-averaged velocity field on the shelf suggests that MAB and SAB waters converge and export to the open ocean near A4. Savidge and Bane (2001) found the strongest innershelf (20 m isobath) convergence between a pair of moorings on either side of Diamond Shoals, while the strongest midshelf (35 m isobath) convergence is between a pair north of the shoals. The mean depth-averaged along-isobath currents at the shelfbreak are



overall convergent except between the pair of Gulf Stream moorings, with the largest convergence between A2 and A3. The mean velocity at A2 rotates about 50° clockwise with increasing depth in the upper 40 m, and then rotates about 20° counterclockwise with depth in the lower 50 m. The surface current has a direction of about 20° clockwise from true east and has a 3.3 cm/s offshore component, which could result in part from an offshore current along the Hatteras Front (Churchill & Gawarkiewicz, 2012). Together with the mean SST, our observations find the Hatteras Front to be near Diamond Shoals over the inner shelf and to extend northeastward over the mid and outer shelf.

The current velocity at A3 is largely affected by the Gulf Stream. The surface current has a direction similar to that at A6 while the bottom current is more like that at A2, which suggests that at A3 the surface layer is dominated by Gulf Stream flow while the bottom layer is largely Shelfbreak Jet. The relatively large offshore current throughout the water column indicates that A3 might be a favored location for the Shelfbreak Jet deflection and enhanced shelf water export.

The current velocity variations are typically several times greater than the mean speed (Figure 1a) or the amplitude of the annual signal at all the moorings except for those dominated by Gulf Stream flow (A6 and A8). Similar to the annual cycle of these current velocities, the magnitudes of the velocity variations also change seasonally. Like the wind stress variations described in Seim et al. (2022), current variations are typically larger in the cool season (mid-September through April) and smaller in the warm season (May–mid-September). The variance of the depth-averaged current velocities in the cool season is nearly twice that in the warm season at the moorings north of Cape Hatteras on the MAB and at the northern shelfbreak. The variance differences at the SAB moorings are not as large, but the current velocity variance in the cool season is also larger than that in the warm season. On the shelf, more than 56% of the current velocity variance is in the weather band (2–10 days), possibly due to frequent extratropical and tropical cyclone passages in this region. The number of cyclones passing the PEACH region is similar in the warm and cool seasons, however, the cyclones in the cool season are much stronger than those in the warm season (personal communication with J. Bane). Furthermore, the cyclone tracks in the cool season are closer to the mooring array than in the warm season. The more intense and closer cyclones in the cool season cause larger current variations.

The wind-driven variability (EOF-1) of the current velocities is along the local isobaths. Overall, it explains more than 40% of the total velocity variance at all 9 moorings. The reconstructed Mode 1 accounts for 50%–70% of the total variance observed by the shelf moorings, 25%–50% at the northern shelfbreak moorings and less than 10% at the Gulf Stream moorings. Wind is the primary driver of the shelf currents. Stronger southward wind (positive PC1) drives stronger equatorward currents and transports more MAB water toward Cape Hatteras, while stronger northward wind (negative PC1) drives stronger poleward currents and transports more SAB water toward Cape Hatteras. The location at which the Shelfbreak Jet deflects to the open ocean is also primarily determined by the wind. Only in cases of southward wind (positive PC1), does the equatorward-flowing Shelfbreak Jet reach the three northern shelfbreak moorings and deflect to the open ocean, converging with the Gulf Stream. By examining the drifter trajectories crossing the 1,000 m isobath, Gawarkiewicz and Linder (2006) identified two primary types of Shelfbreak Jet entrainment in the Gulf Stream: a rapid and abrupt turn within 20 km of Cape Hatteras, and a slow passage across the slope region to the Gulf Stream well north of Hatteras (20–100 km), with a gradual turn. The rapid and abrupt entrainment resembles the conditionally averaged surface velocity patterns in conditions 1 and 2 when PC1 is positive, while the slow and gradual entrainment agrees well with conditions 3 and 4 (negative PC1). In condition 1, the onshore movement of the Gulf Stream promotes the convergence at the shelfbreak and the Shelfbreak Jet can reach further south and make an abrupt turn when encountering the Gulf Stream.

Approaching Cape Hatteras, the Gulf Stream's lateral position varies as it moves onshore and offshore due to meander propagation, transport variations (Andres, 2021), and eddy activity (Cronin, 1996; Glenn & Ebbesmeyer, 1994). The Gulf Stream-driven variability (EOF-2) is also mostly along local isobaths like EOF-1 but shows a converging pattern toward Cape Hatteras both on the shelf and along the shelfbreak. Savidge and Bane (2001) highlighted the clear correlation between the Gulf Stream variability and the along-shelf transport convergence off Cape Hatteras for the first time. However, their results mainly demonstrated the effects of the Gulf Stream lateral position on shelf transport convergence north of Cape Hatteras, as their Gulf Stream position proxy was at a mooring close to The Point (Figure 8d), and the corresponding transport convergence was computed between two mooring lines north of Cape Hatteras. In our study, the velocities with strong Gulf Stream features were measured upstream of the Point off Raleigh Bay, and EOF-2 shows the strong cross-shelf

component south of Diamond Shoals on the SAB. In the sensitivity analysis, the strong cross-shelf component in EOF-2 moves to the north of Diamond Shoals on the MAB, when increased lags were applied to the Gulf Stream velocities at A6 and A8 (Figure 8). The Gulf Stream reference location of the 25-hr lagged A6 velocity and 50-hr lagged A8 velocity is close to the location of the Gulf Stream proxy in Savidge and Bane (2001) (Figure 8d). Accordingly, the shelf convergence under this circumstance occurs between A4 and B1, which are approximately at the two northern mooring lines in Savidge and Bane (2001). Together, this suggests that the location of shelf water export could be attributed to the Gulf Stream meander processes. The conditional averaged SST and surface velocity show that the shelf water flows offshore near the Gulf Stream meander crest, which further suggests that as a Gulf Stream meander propagates downstream, the shelf water would be exported at the crest.

The shelf water export in this region is episodic and largely event-driven (Churchill & Gawarkiewicz, 2012; Pietrafesa et al., 2002; Savidge & Savidge, 2014; Todd, 2020). The type of shelf water exported depends on whether it is MAB or SAB shelf water that is available inshore of a Gulf Stream meander crest. When the MAB shelf water is pushed south of Diamond Shoals by a strong southward wind, it is closer to the Gulf Stream and can then be exported by a Gulf Stream-driven offshore flow. Otherwise, this process will export the local SAB shelf water to the open ocean. When the Gulf Stream moves onshore (positive PC2), southward wind (positive PC1) occurs more in the winter and northward wind (negative PC1) occurs more in the summer. This allows for more MAB shelf water to be exported in the winter and more SAB shelf water to be exported in the summer, as demonstrated in Savidge and Savidge (2014). The larger volume of shelf water carried by the Shelfbreak Jet is another source of shelf water export in this region. During southward wind (positive PC1), the Shelfbreak Jet is deflected offshore in close proximity to Cape Hatteras, often with an abrupt turn into the Gulf Stream. This seaward turn exports the shelf water to the edge of the Gulf Stream, which can be an important source of “Ford Water” (Church, 1937; Ford et al., 1952; Kupferman & Garfield, 1977; Lillibridge et al., 1990), exported MAB shelf water entrained along the northern edge of the Gulf Stream. When the wind is northward (negative PC1), the Shelfbreak Jet detachment occurs generally well north of the PEACH region and exports the shelf water to the Slope Sea.

Despite the wind-driven and Gulf Stream-driven variability of the current velocity on the shelf, the location of the shelf convergence is well constrained between the northernmost shelf mooring B1 and southernmost shelf mooring B2. Pressure gradients from density gradients and sea surface slopes could contribute to the mean converging flow pattern being contained in the vicinity of Cape Hatteras. Given the approximate thermal wind balance at the interior layer for the A4 mooring that was established above, the mean density gradients are inferred using the vertical shear of the current velocities at the shelf moorings and northern shelfbreak moorings. The large negative vertical shear of along-shelf flow would suggest that the water offshore of A4 is denser than the water inshore through the entire water column (positive cross-shelf density gradient). Freshwater export from the Chesapeake Bay and the North Carolina sounds could contribute to the positive cross-shelf density gradient (Savidge & Bane, 2001). Extending the assumption of a thermal wind balance to the interior layer at all the shelf moorings, the vertical shear of the alongshelf currents and the inferred cross-shelf density gradients at B1 and B2 averaged between 10 and 20 m both have magnitudes which are about 1/4 of the that at A4. The sign of the vertical shear at B2 is opposite that at A4 and B1, suggesting the water offshore of B2 is slightly less dense than that inshore, which could be explained by the presence of less dense Gulf Stream water on the outer shelf of the SAB (Lee et al., 1991). As the shelf narrows from B2 to A7, the vertical shear and inferred cross-shelf density gradient at A7 is near zero. At the shelfbreak, the along-shelf vertical shear at A1 and A2 is consistent throughout the water column, but with opposite signs, which suggests opposite cross-shelf density gradients at the two moorings, assuming geostrophy. Water offshore of A1 is denser than water inshore. Water offshore of A2 is less dense than water inshore; the same holds true at A3, but with a much larger density gradient. Together, this suggests that with similar shelf water inshore of the three moorings, the water offshore becomes less dense from north to south. This configuration agrees with the mean density field measured by the Spray gliders offshore of the northern shelfbreak mooring array (A1, A2, and A3) in the Slope Sea during PEACH (Todd, 2020).

In addition to the along-shelf density gradient term, an along-shelf surface slope of  $-3.3 \times 10^{-7}$  (increasing elevation to the south) would be required to drive the 4.7 cm/s mean offshore current in the interior layer at A4. The along-shelf sea surface slope may also be negative on the SAB shelf, estimated to be  $-0.67 \times 10^{-7}$  for the summer/fall period and  $-1.63 \times 10^{-7}$  for the winter/spring period at the Georgia coast (Atkinson et al., 1983). From south to north on the entire SAB shelf, model-based climatological surface elevation along the 70-m isobath determined the mass field was estimated to mostly decrease, an exception being at the Charleston Bump

where the along-shelf surface slope becomes steeper in the winter (Blanton et al., 2003). The surface slope is not geographically uniform, being steeper toward the southern and northern ends of the SAB shelf (Blanton et al., 2003). As a result, the slope should be negative in Raleigh Bay with a magnitude larger than that at the Georgia coast. On the MAB shelf, the along-shelf sea surface slope turns positive, but its magnitude is only on the order of  $10^{-8}$  (Lentz, 2008a; Xu & Oey, 2011), an order of magnitude smaller than that estimated at A4. Along the 30 m isobath around Cape Hatteras, the sea level reaches its minimum value at the southern end of the MAB, between B1 and A4. The 30-m isobath at A4 is oriented approximately N–S and the Gulf Stream's mean path is oriented about 45° clockwise of that. The Gulf Stream proximity to the mid shelf south of A4 and its more offshore position north of it could contribute to the steep along-shelf surface slope at A4. When a Gulf Stream meander passes by, a negative along-shelf surface slope will be superimposed at the shelfbreak and drive an offshore flow at the leading edge of the meander crest.

## 5. Summary

The PEACH observations further illustrate the complexity of the circulation near Cape Hatteras. From the 18-month current observations at 9 PEACH mooring sites, a converging mean flow pattern was observed on the shelf and along the shelfbreak. The mean depth-averaged flows are mostly aligned with local isobaths and oriented toward Cape Hatteras. On the shelf, the mean flow has a strong cross-shelf component at the mooring just north of Cape Hatteras, where the MAB and SAB waters converge and export to the open ocean. The mean convergence and offshore current are possibly driven by the mean along-shelf sea surface slope. Along the shelfbreak, the mean convergence is between the equatorward flowing Shelfbreak Jet and the poleward flowing Gulf Stream. The Shelfbreak Jet deflects to the ocean open near The Point. The Hatteras Front is typically found just north of Diamond Shoals with a mean off-shore flow on both the mid- and outer-shelf (A4 and A3).

On the shelf, the along-shelf velocities are well correlated. North of Cape Hatteras, the shelf flow and shelfbreak flow are more correlated than to the south. Along the shelfbreak south of Cape Hatteras, the lagged correlation between along-isobath velocities is large, due to propagating Gulf Stream meanders. The cross-shelf velocities have much lower correlation compared to the along-shelf flows. The annual variations of the depth-averaged current velocities are consistent at all 9 moorings. And the larger current velocity variations in the cool season are associated with more intense closer cyclones relative to those in the warm season.

The EOF analysis yields two prominent spatial variations in the velocity field. One shows a wind-driven along-shelf flow pattern (EOF-1), the other a Gulf Stream-driven convergent flow pattern (EOF-2). Conditionally averaged sea-surface temperature and high-frequency radar-measured surface currents based on PC1 and PC2 provide a rich 2-D representation of the wind-driven and Gulf Stream-driven features.

- The southward extent of the Shelfbreak Jet is primarily influenced by the wind but secondarily by the Gulf Stream.
- The Gulf Stream meander crest propagation from offshore of Raleigh Bay to The Point is associated with convergent shelf flow and presumably export.
- The SAB occupies Raleigh Bay most of the time and is often exported near a Gulf Stream meander crest.
- Strong southward wind events appear to drive the MAB shelf water southward, where it encounters the edge of the Gulf Stream, to become entrained and exported to the open ocean.
- The seasonal variation in shelf water export off Cape Hatteras may be related to the combined effects of Gulf Stream-driven shelf convergence and varying wind-driven shelf transport.

## Data Availability Statement

Processed PEACH ADCP and CTD data (Haines, Seim, Muglia, et al., 2022) are available at: <https://doi.org/10.5281/zenodo.6383218>. PEACH wind stress data (Haines, Seim, & Bane, 2022) are available at: <https://doi.org/10.5281/zenodo.6383242>. The combine High Frequency Radar data (Haines, Muglia, Savidge, et al., 2022) are available at: <https://doi.org/10.5281/zenodo.7044816>. PEACH CPIES data (Andres, 2021) are available at: <http://doi.org/10.5281/zenodo.4793504>. Sea surface temperature (SST) was measured by NOAA's Advanced Very High Resolution Radiometer (AVHRR), with spatial resolution of 1 km and was obtained from the Mid-Atlantic Regional Association Coastal Ocean Observing System (MARACOOS) THREDDS server (<https://tds.maracoos.org>).

[org/thredds/catalog/ARCHIVE-SST.html](https://org.thredds/catalog/ARCHIVE-SST.html)). Sea surface height data used here are level-4 reprocessed observations available from Copernicus Marine Service (SEALEVEL\_GLO\_L4\_REP\_OBSERVATIONS\_008\_047).

### Acknowledgments

This research was funded by the National Science Foundation (Grants OCE-1558920 to University of North Carolina at Chapel Hill, OCE-1559476 to Skidaway Institute of Oceanography and OCE-1558521 to Woods Hole Oceanographic Institution) as part of PEACH. We acknowledge and thank Sara Haines for the processing and QC of the mooring and HFR data, and we thank the PEACH group for helpful discussions and for their support. Paper preparation and finalization took place while D. Savidge was serving at the US National Science Foundation.

### References

- Andres, M. (2016). On the recent destabilization of the Gulf Stream path downstream of Cape Hatteras. *Geophysical Research Letters*, 43(18), 9836–9842. [https://doi.org/10.1002/2016GL069966@10.1002/\(ISSN\)1944-8007.2016GRLEDHIGH](https://doi.org/10.1002/2016GL069966@10.1002/(ISSN)1944-8007.2016GRLEDHIGH)
- Andres, M. (2020). Processes driving exchange at Cape Hatteras (PEACH) PIESS and AP technical report—Part 1. *Zenodo*. <https://doi.org/10.5281/zenodo.4793402>
- Andres, M. (2021). Spatial and temporal variability of the Gulf Stream near Cape Hatteras. *Journal of Geophysical Research: Oceans*, 126(9), e2021JC017579. <https://doi.org/10.1029/2021JC017579>
- Archer, M. R., Roughan, M., Keating, S. R., & Schaeffer, A. (2017). On the variability of the East Australian Current: Jet structure, meandering, and influence on shelf circulation. *Journal of Geophysical Research: Oceans*, 122(11), 8464–8481. <https://doi.org/10.1002/2017JC013097>
- Atkinson, L. P., Lee, T. N., Blanton, J. O., & Chandler, W. S. (1983). Climatology of the southeastern United States continental shelf waters. *Journal of Geophysical Research*, 88(C8), 4705–4718. <https://doi.org/10.1029/JC088iC08p04705>
- Berger, T. J., Blanton, J. O., Boicourt, W. C., Churchill, J. H., Hamilton, P., Watts, D. R., & Wayland, R. J. (1995). A physical oceanographic field program offshore of North Carolina. Report MMS, 94, p. 463.
- Blanton, B. O., Aretxabaleta, A., Werner, F. E., & Seim, H. E. (2003). Monthly climatology of the continental shelf waters of the South Atlantic Bight. *Journal of Geophysical Research*, 108, 3264. <https://doi.org/10.1029/2002JC001609>
- Chapman, D. C., & Beardsley, R. C. (1988). On the origin of shelf water in the middle Atlantic bight. *Journal of Physical Oceanography*, 19(3), 384–391. [https://doi.org/10.1175/1520-0485\(1989\)019<0384:otoosw>2.0.co;2](https://doi.org/10.1175/1520-0485(1989)019<0384:otoosw>2.0.co;2)
- Church, P. E. (1937). Temperatures of the western North Atlantic from thermograph records. *Association d'Océanographie Physique Internationale Union of Geodesy and Geophysics*, 4, 1–32.
- Churchill, J. H., & Berger, T. J. (1998). Transport of middle Atlantic bight shelf water to the Gulf Stream near Cape Hatteras. *Journal of Geophysical Research*, 103(C13), 30605–30621. <https://doi.org/10.1029/98JC01628>
- Churchill, J. H., & Gawarkiewicz, G. G. (2012). Pathways of shelf water export from the Hatteras shelf and slope. *Journal of Geophysical Research*, 117(C8), C08023. <https://doi.org/10.1029/2012JC007995>
- Churchill, J. H., & Gawarkiewicz, G. G. (2014). Shelf water and chlorophyll export from the Hatteras slope and outer shelf. *Journal of Geophysical Research: Oceans*, 119(7), 4291–4304. <https://doi.org/10.1002/2014JC009809>
- Codiga, D. L. (2011). Investigating tidal influences on subtidal estuary-coast exchange using observations and numerical simulations. Retrieved from <http://www.po.gso.uri.edu/pub/downloads/codiga/pubs/2011Codiga-UTide-Report.pdf>
- Cronin, M. (1996). Eddy-mean flow interaction in the Gulf Stream at 68°W. Part II: Eddy forcing on the time-mean flow. *Journal of Physical Oceanography*, 26(10), 2132–2151. [https://doi.org/10.1175/1520-0485\(1996\)026<2132:EMFIIT>2.0.CO;2](https://doi.org/10.1175/1520-0485(1996)026<2132:EMFIIT>2.0.CO;2)
- Csanady, G. T., & Hamilton, P. (1988). Circulation of slope water. *Continental Shelf Research*, 8(5–7), 565–624. [https://doi.org/10.1016/0278-4343\(88\)90068-4](https://doi.org/10.1016/0278-4343(88)90068-4)
- Edson, J. B., Jampana, V., Weller, R. A., Bigorre, S. P., Plueddemann, A. J., Fairall, C. W., et al. (2013). On the exchange of momentum over the open ocean. *Journal of Physical Oceanography*, 43(8), 1589–1610. <https://doi.org/10.1175/JPO-D-12-01073.1>
- Edwards, C. R., & Seim, H. E. (2008). Complex EOF analysis as a method to separate barotropic and baroclinic velocity structure in shallow water. *Journal of Atmospheric and Oceanic Technology*, 25(5), 808–821. <https://doi.org/10.1175/2007JTECHO562.1>
- Fairall, C. W., Bradley, E. F., Hare, J. E., Grachev, A. A., & Edson, J. B. (2003). Bulk parameterization of air–sea fluxes: Updates and verification for the COARE algorithm. *Journal of Climate*, 16(4), 571–591. [https://doi.org/10.1175/1520-0442\(2003\)016<0571:BPOASF>2.0.CO;2](https://doi.org/10.1175/1520-0442(2003)016<0571:BPOASF>2.0.CO;2)
- Ford, W. L., Longard, J. R., & Banks, R. E. (1952). On the nature, occurrence and origin of cold low salinity water along the edge of the Gulf Stream. *Journal Marine Science*, 11, 281–293.
- Forsyth, J., Andres, M., & Gawarkiewicz, G. (2020). Shelfbreak jet structure and variability off New Jersey using ship of opportunity data from the CMV oleander. *Journal of Geophysical Research: Oceans*, 125(9), e2020JC016455. <https://doi.org/10.1029/2020JC016455>
- Fratantoni, P. S., & Pickart, R. S. (2007). The western North Atlantic shelfbreak current system in summer. *Journal of Physical Oceanography*, 37(10), 2509–2533. <https://doi.org/10.1175/JPO3123.1>
- Gawarkiewicz, G., Churchill, J., Bahr, F., Linder, C., & Marquette, C. (2008). Shelfbreak frontal structure and processes north of Cape Hatteras in winter. *Journal of Marine Research*, 66(6), 775–799. <https://doi.org/10.1357/00224008788064595>
- Gawarkiewicz, G., & Linder, C. A. (2006). Lagrangian flow patterns north of Cape Hatteras using near-surface drifters. *Progress in Oceanography*, 70(2–4), 181–195. <https://doi.org/10.1016/j.pocan.2006.03.020>
- Glenn, S. M., & Ebbesmeyer, C. C. (1994). Observations of Gulf Stream frontal eddies in the vicinity of Cape Hatteras. *Journal of Geophysical Research*, 99(C3), 5047–5055. <https://doi.org/10.1029/93JC02787>
- Haines, S., Muglia, M., Bahr, F., Hogue, B., Taylor, P. I., DeSimone, N., & Matthias, G. (2022). Mooring data report for the processes driving exchange at Cape Hatteras (PEACH) program. <https://doi.org/10.5281/ZENODO.6390566>
- Haines, S., Muglia, M., Savidge, D., Han, L., & Seim, H. (2022). Processed high frequency radar (HFR) surface current data for the processes driving exchange at Cape Hatteras (PEACH) program (level 2—v1.0) [Dataset]. *Zenodo*. <https://doi.org/10.5281/zenodo.7044816>
- Haines, S., Seim, H., & Bane, J. (2022). Processed buoy and bulk heat flux data for the processes driving exchange at Cape Hatteras (PEACH) program (level 2—v1.0) [Dataset]. *Zenodo*. <https://doi.org/10.5281/zenodo.6383242>
- Haines, S., Seim, H., & Muglia, M. (2017). Implementing quality control of high-frequency radar estimates and application to Gulf Stream surface currents. *Journal of Atmospheric and Oceanic Technology*, 34(6), 1207–1224. <https://doi.org/10.1175/JTECH-D-16-0203.1>
- Haines, S., Seim, H., Muglia, M., Gawarkiewicz, G., & Savidge, D. (2022). Processed ADCP and CTD data for the processes driving exchange at Cape Hatteras (PEACH) program (level 2—v1.0) [Dataset]. *Zenodo*. <https://doi.org/10.5281/zenodo.6383219>
- Han, L., Seim, H., Bane, J., Todd, R. E., & Muglia, M. (2021). A shelf water cascading event near Cape Hatteras. *Journal of Physical Oceanography*, 51(6), 2021–2033. <https://doi.org/10.1175/JPO-D-20-0156.1>
- Hersbach, H., Bell, B., Berrisford, P., Biavati, G., Horányi, A., Muñoz Sabater, J., et al. (2018). ERA5 hourly data on single levels from 1979 to present. In *Copernicus Climate Change Service (C3S)*. Climate Data Store (CDS).
- Kaihatu, J. M., Handler, R. A., Marmorino, G. O., & Shay, L. K. (1998). Empirical orthogonal function analysis of ocean surface currents using complex and real-vector methods. *Journal of Atmospheric and Oceanic Technology*, 15(4), 927–941. [https://doi.org/10.1175/1520-0426\(1998\)015<0927:eofaoo>2.0.co;2](https://doi.org/10.1175/1520-0426(1998)015<0927:eofaoo>2.0.co;2)



- Kupferman, S. L., & Garfield, N. (1977). Transport of low-salinity water at the slope water-Gulf Stream boundary. *Journal of Geophysical Research*, 82(24), 3481–3486. <https://doi.org/10.1029/JC082i024p03481>
- Lee, T. N., Yoder, J. A., & Atkinson, L. P. (1991). Gulf Stream frontal eddy influence on productivity of the southeast U.S. continental shelf. *Journal of Geophysical Research*, 96(C12), 22191–22205. <https://doi.org/10.1029/91JC02450>
- Lentz, S. J. (2008a). Observations and a model of the mean circulation over the middle Atlantic bight continental shelf. *Journal of Physical Oceanography*, 38(6), 1203–1221. <https://doi.org/10.1175/2007JPO3768.1>
- Lentz, S. J. (2008b). Seasonal variations in the circulation over the Middle Atlantic Bight continental shelf. *Journal of Physical Oceanography*, 38(7), 1486–1500. <https://doi.org/10.1175/2007JPO3767.1>
- Lillibridge, J. L., Hitchcock, G., Rossby, T., Lessard, E., Mork, M., & Golmen, L. (1990). Entrainment and mixing of shelf/slope waters in the near-surface Gulf Stream. *Journal of Geophysical Research*, 95(C8), 13065. <https://doi.org/10.1029/jc095ic08p13065>
- Linder, C. A., & Gawarkiewicz, G. (1998). A climatology of the shelfbreak front in the Middle Atlantic Bight. *Journal of Geophysical Research*, 103(C9), 18405–18423. <https://doi.org/10.1029/98JC01438>
- Mantovanelli, A., Heron, M. L., Heron, S. F., & Steinberg, C. R. (2012). Relative dispersion of surface drifters in a barrier reef region. *Journal of Geophysical Research: Oceans*, 117, C11016. <https://doi.org/10.1029/2012JC008106>
- North, G. R., Bell, T. L., Cahalan, R. F., & Moeng, F. J. (1982). Sampling errors in the estimation of empirical orthogonal functions. *Monthly Weather Review*, 110(7), 699–706. [https://doi.org/10.1175/1520-0493\(1982\)110<0699:SEITEO>2.0.CO;2](https://doi.org/10.1175/1520-0493(1982)110<0699:SEITEO>2.0.CO;2)
- Percival, D. B., & Walden, A. T. (1993). *Spectral analysis for physical applications*. Cambridge University Press. <https://doi.org/10.1017/CBO9780511622762>
- Pietrafesa, L. J., Flagg, C. N., Xie, L., Weatherly, G. L., & Morrison, J. M. (2002). The winter/spring 1996 OMP current, meteorological, sea state and coastal sea level fields. *Deep Sea Research Part II: Topical Studies in Oceanography*, 49(20), 4331–4354. [https://doi.org/10.1016/S0967-0645\(02\)00166-2](https://doi.org/10.1016/S0967-0645(02)00166-2)
- Savidge, D. K. (2004). Gulf Stream meander propagation past Cape Hatteras. *Journal of Physical Oceanography*, 34(9), 2073–2085. [https://doi.org/10.1175/1520-0485\(2004\)034<2073:gsmppc>2.0.co;2](https://doi.org/10.1175/1520-0485(2004)034<2073:gsmppc>2.0.co;2)
- Savidge, D. K., & Austin, J. A. (2007). The Hatteras Front: August 2004 velocity and density structure. *Journal of Geophysical Research*, 112(C7), C07006. <https://doi.org/10.1029/2006JC003933>
- Savidge, D. K., & Bane, J. M. (2001). Wind and Gulf Stream influences on along-shelf transport and off-shelf export at Cape Hatteras, North Carolina. *Journal of Geophysical Research*, 106(C6), 11505–11527. <https://doi.org/10.1029/2000JC000574>
- Savidge, D. K., & Savidge, W. B. (2014). Seasonal export of South Atlantic bight and mid-Atlantic bight shelf waters at Cape Hatteras. *Continental Shelf Research*, 74, 50–59. <https://doi.org/10.1016/j.csr.2013.12.008>
- Seim, H., Savidge, D., Andres, M., Bane, J., Edwards, C., Gawarkiewicz, G., et al. (2022). Overview of the processes driving exchange at Cape Hatteras program. *Oceanography*. <https://doi.org/10.5670/oceanog.2022.205>
- Thomson, R. E., & Emery, W. J. (2014). *Data analysis methods in physical oceanography* (3rd ed., pp. 1–716). Newnes. <https://doi.org/10.1016/C2010-0-66362-0>
- Todd, R. E. (2020). Export of Middle Atlantic Bight shelf waters near Cape Hatteras from two years of underwater glider observations. *Journal of Geophysical Research: Oceans*, 125(4), e2019JC016006. <https://doi.org/10.1029/2019JC016006>
- Townsend, D. W., Thomas, A. C., Mayer, L. M., Thomas, M. A., & Quinlan, J. A. (2006). Chapter 5. *Oceanography of the northwest Atlantic continental shelf* (Vol. 14).
- Venegas, S. A. (2001). *Statistical methods for signal detection in climate*. Danish center for Earth system science. DCESS Report 2. University of Copenhagen.
- Verity, P. G., Bauer, J. E., Flagg, C. N., DeMaster, D. J., & Repeta, D. J. (2002). The Ocean Margins Program: An interdisciplinary study of carbon sources, transformations, and sinks in a temperate continental margin system. *Deep-Sea Research Part II Topical Studies in Oceanography*, 49(20), 4273–4295. [https://doi.org/10.1016/S0967-0645\(02\)00120-0](https://doi.org/10.1016/S0967-0645(02)00120-0)
- Xu, F.-H., & Oey, L.-Y. (2011). The origin of along-shelf pressure gradient in the Middle Atlantic Bight. *Journal of Physical Oceanography*, 41(9), 1720–1740. <https://doi.org/10.1175/2011JPO4589.1>